

**Thermodynamic models for a concentration and electric field
dependent susceptibility in liquid electrolytes**

Manuel Landstorfer, Rüdiger Müller

submitted: December 17, 2021

Weierstrass Institute
Mohrenstr. 39
10117 Berlin
Germany
E-Mail: manuel.landstorfer@wias-berlin.de
ruediger.mueller@wias-berlin.de

No. 2906
Berlin 2021



2020 *Mathematics Subject Classification.* 65N30, 78A57, 80A17, 35Q61.

Key words and phrases. Electrochemistry, double layer, dielectric susceptibility, dielectric decrement, dielectric saturation.

This work was supported by the German Research Foundation (DFG) under the Germany's Excellence Strategy – The Berlin Mathematics Research Center MATH+ (EXC-2046/1) in project AA2-6. We thank Wolfgang Dreyer for many helpful discussions and suggestions.

Edited by
Weierstraß-Institut für Angewandte Analysis und Stochastik (WIAS)
Leibniz-Institut im Forschungsverbund Berlin e. V.
Mohrenstraße 39
10117 Berlin
Germany

Fax: +49 30 20372-303
E-Mail: preprint@wias-berlin.de
World Wide Web: <http://www.wias-berlin.de/>

Thermodynamic models for a concentration and electric field dependent susceptibility in liquid electrolytes

Manuel Landstorfer, Rüdiger Müller

Abstract

The dielectric susceptibility χ is an elementary quantity of the electrochemical double layer and the associated Poisson equation. While most often χ is treated as a material constant, its dependency on the salt concentration in liquid electrolytes is demonstrated by various bulk electrolyte experiments. This is usually referred to as dielectric decrement. Further, it is theoretically well accepted that the susceptibility declines for large electric fields. This effect is frequently termed dielectric saturation. We analyze the impact of a variable susceptibility in terms of species concentrations and electric fields based on non-equilibrium thermodynamics. This reveals some non-obvious generalizations compared to the case of a constant susceptibility. In particular the consistent coupling of the Poisson equation, the momentum balance and the chemical potentials functions are of ultimate importance. In a numerical study, we systematically analyze the effects of a concentration and field dependent susceptibility on the double layer of a planar electrode|electrolyte interface. We compute the differential capacitance and the spatial structure of the electric potential, solvent concentration and ionic distribution for various non-constant models of χ .

1 Introduction

When an electrode-electrolyte interface is charged, thin boundary layers arise where the electric charge is accumulated, in the electrolyte due to ionic charges and in the electrode due to variations of the electron charge density. In this *electrochemical double layer* the local ion concentrations deviate from their respective bulk concentration and strong electric fields are present. It might seem surprising that the electrochemical double layer is still not sufficiently theoretically understood, even in most simple situations, cf. [46]. The purpose of macroscopic continuum models is to integrate the effects of the double layer in a consistent way into applications. In the vast majority of the continuum models, the dielectric susceptibility χ –also referred to as the static relative permittivity– is treated as a constant, mostly for the sake of simplicity. But, e.g. in aqueous solutions, χ is known to depend on the electrolyte concentration, cf. e.g. [30, 11, 38] and see Fig. 1. For pure water at room temperature the susceptibility is $\chi_S \approx 80$ and for many salts a linear *dielectric decrement* of the form

$$\chi = \chi_S - d \cdot c \quad (+ \text{h. o. t.}) \quad (1.1)$$

can be experimentally observed, at least in solutions up to concentrations of $c \approx 2 \text{ mol L}^{-1}$, cf. [6, 38]. For more concentrated solutions, higher order terms can be added to (1.1), e.g. a term proportional to c^2 is used in [42], and a term proportional to $c^{3/2}$ can be found in [11, 1]. However, we want to remark that in the presence ion pair formation or incomplete dissociation of the electrolyte, already a linear approach like (1.1) can provide non-linear dependence of the susceptibility with respect to the total salt concentration in qualitative agreement with Fig. 1, cf. Fig. 6. Moreover, it is well accepted that the strong electric field inside the double layer causes alignment of the microscopic dipoles to the field, whereby

the susceptibility is reduced [27, 9, 37]. This concept of *dielectric saturation* is based on the theory of [15, 43] and extensions. We are not aware of any direct measurement of the dielectric saturation, however experimental results of [47] suggest that at the interface of water there are spatial profiles of χ which seem compatible with this concept, see Fig. 1.

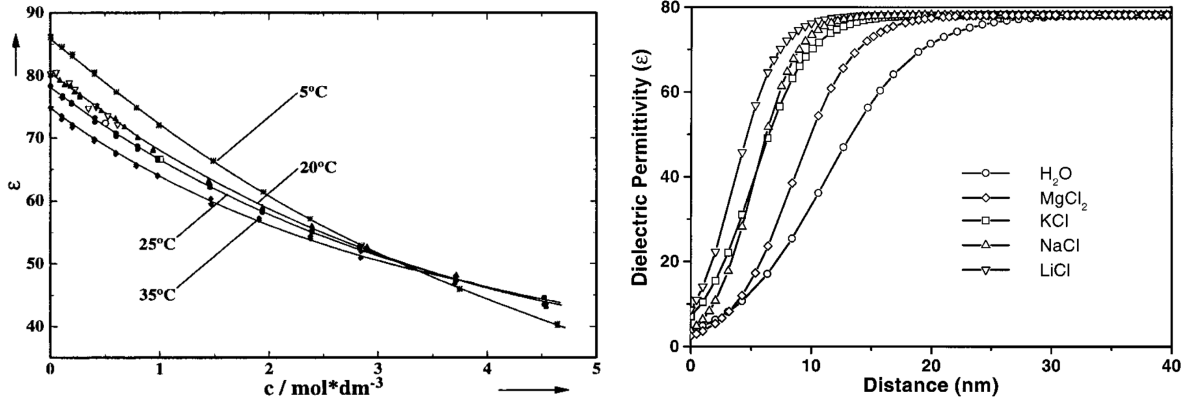


Figure 1: Left: concentration dependent susceptibility (Fig. 2 of [11]). Right: profile of χ in the double layer (Fig. 9 of [47]).

It should be expected that both, dielectric decrement as well as dielectric saturation, have considerable influence on the double layer at electrode|electrolyte interface and on the fundamental macroscopic electrochemical relation between electrode charge and potential, which is equivalently expressed in terms of the differential capacitance of the interface. Measurements of the differential capacitance of (well defined) planar single crystal surfaces, cf. [49], yield highly reproducible results that are well suited for the validation of mathematical models of the double layer. For an applied potential $E - E^{\text{ref}}$ relative to a reference electrode, the (boundary layer contribution of the) differential capacitance is defined in the absence of specific adsorption as

$$C^{\text{BL}}(E - E^{\text{ref}}) = \frac{d}{dE} Q^{\text{BL}}(E - E^{\text{ref}}) \quad \text{with} \quad Q^{\text{BL}}(E - E^{\text{ref}}) = - \int_{\Omega^{\text{BL}}} q(z) dz, \quad (1.2)$$

where q is the free charge density in the electrolyte, Ω^{BL} denotes a suitable spatial domain for the boundary layer in front of the electrode and Q^{BL} is the charge density of the electrode surface which is compensated by the boundary layer charge. The free charge density q in the electrolyte is determined by the Poisson equation for the electric potential φ , i.e.

$$- \text{div}((1 + \chi)\epsilon_0 \nabla \varphi) = q. \quad (1.3)$$

In order to solve (1.3), constitutive laws for χ and q need to be provided by means of mathematical modelling of the double layer. On the left hand side of (1.3), it is very tempting to assume a constant susceptibility χ across the whole layer. For the right hand side, the most simple model is the Gouy-Chapman (GC) model based on the assumption of a Boltzmann distribution of ions in strongly diluted solutions, [8]. Many extensions and generalizations to this most simple setting have been proposed in the literature but we postpone the review and discussion of various models and approaches to the Section 3.1 below.

The purpose of this paper is, to derive on the basis of the general non-equilibrium thermodynamic framework [19, 34, 20] a complete and consistent model with constitutive equations that take dielectric decrement as well as dielectric saturation into account. While in the case of constant susceptibility the

electrochemical potentials can be split into the electric potential governed by the Maxwell equations and a chemical potential independent of the electric field, the situation changes if χ depends on the local electrolytic species concentrations and the chemical potentials also depend on the electric potential. This was noted first by [45, eqn. (5.39)], where the chemical potentials are modified by a term quadratic in the electric field. The non-constant susceptibility and the possibly field dependent chemical potentials show up in the balances of (partial) mass and momentum and these equations have to be consistently solved in order to determine the free charge density in the Poisson equation. This way non-obvious extensions to established models from the literature are necessary. The properties of the obtained mathematical model are then analyzed in a numerical study. We illustrate the consequences of dielectric decrement and dielectric saturation on the double layer and the resulting differential capacitance of the interface.

We remark that χ is typically measured using high-frequency techniques, cf. e.g. [11], and in the literature there is some controversy about a dynamic contribution to the static dielectric constant with several studies showing the presence and others the absence of the dynamic contribution, cf. e.g. [12] and the literature cited therein. In the following, the susceptibility is treated as an equilibrium parameter.

2 Continuum model with non-constant susceptibility

In the following modeling, we restrict our considerations to the quasi-electrostatic and isothermal case, where the electric field can be represented by the electric potential as $\mathbf{E} = -\nabla\varphi$ and the temperature T enters the equations only as a constant parameter. Since we are only interested in the case of a scalar susceptibility χ , i.e. where the vector of polarization can be written as $\mathbf{P} = \chi\epsilon_0\mathbf{E}$, we assume that $\mathbf{P} \otimes \mathbf{E}$ defines a symmetric tensor. In the following, we neglect gravitation and restrict the presentation to planar interfaces with no tangential transport on the surface.

2.1 Description of reacting mixtures

The electrolyte is modeled as a general mixture of several different constituents. These constituents can be e.g. a solvent, ions, ion pairs or larger complexes. To refer to the different species, we introduce an index set \mathcal{I} and typically use an index $\alpha \in \mathcal{I}$. The constituents have molecular masses m_α and carry a charge $z_\alpha e_0$, where e_0 is the elementary charge. Moreover, to account for the size of the molecules, we assign to each constituent a specific volume v_α^E . At each point in space, we denote the number density of species by n_α for $\alpha \in \mathcal{I}$. The mass density ρ and free charge density q of the electrolyte are

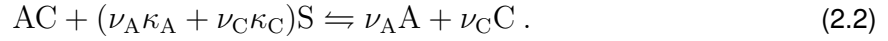
$$\rho = \sum_{\alpha \in \mathcal{I}} m_\alpha n_\alpha \quad \text{and} \quad q = e_0 \sum_{\alpha \in \mathcal{I}} z_\alpha n_\alpha . \quad (2.1)$$

In the following we consider only a single type of solvent species, typically referred to by the index $\alpha = S$ or $\alpha = 0$ and we assume here $z_0 = 0$, but emphasize that our model framework can easily be extended to mixtures of solvents.

In many electrolytes, the ions are assumed to bind a certain number of solvent molecules to form larger compounds that are called *solvated ions*. This solvation can be described by a solvation reaction where e.g. a bare unsolvated anion, denoted by \tilde{A} , binds κ_A solvent molecules S to form the solvated anion denoted by A . Analogously, a bare unsolvated cation C_0 , binds κ_C solvent molecules S to form the solvated cation C . Here κ_α , for $\alpha \in \{A, C\}$, are called the solvation numbers. Since mass

is conserved during the solvation, the mass of a solvated anion A is $m_A = m_{\tilde{A}} + \kappa_A m_S$ and an analogous identity holds for the mass of the solvated cation.

The solvation is in particular important, because the bound solvent molecules do not contribute to the entropy of mixing. In the following, we assume for simplicity that all ions are solvated. Another important aspect of the solvation is the impact on the formation of undissociated ion pairs in solution. Consider an ion pair AC which dissociates into ν_A anions and ν_C cations. Then, the net reaction of the dissociation and solvation is



Under the assumption that the electrolyte consists exclusively of the species from the index set $\mathcal{I} = \{A, C, AC, S\}$, (2.2) implies an upper limit for the ion concentration such that complete dissociation into solvated ions is possible [33]. In more concentrated electrolytes, where not enough solvent molecules are left to proceed with the dissociation reaction, ion pairs AC remain constituents of the mixture, which have to be accounted for.

More general, $M \geq 1$ reactions between the species A_α for $\alpha \in \mathcal{I}$ can be considered, with (2.2) being one of them. Each of the reactions has to conserve mass and charge. Therefore, we introduce the stoichiometric coefficients $\nu_{\alpha,m}$ for $\alpha \in \mathcal{I}$ and $1 \leq m \leq M$ to write

$$\sum_{\alpha \in \mathcal{I}} \nu'_{\alpha,m} A_\alpha \rightleftharpoons \sum_{\alpha \in \mathcal{I}} \nu''_{\alpha,m} A_\alpha \quad \text{with } \nu_{\alpha,m} := \nu''_{\alpha,m} - \nu'_{\alpha,m}, \quad \sum_{\alpha \in \mathcal{I}} \nu_{\alpha,m} m_\alpha = 0 \quad \text{and} \quad \sum_{\alpha \in \mathcal{I}} \nu_{\alpha,m} z_\alpha = 0. \quad (2.3)$$

2.2 Balance equations and general constitutive model

We first introduce balance equations that are universal, i.e. independent of the considered material. However, these equations contain material dependent constitutive quantities which need appropriate modeling. Then, by application of an entropy principle, cf. [20], we restrict the constitutive equations to guarantee non-negative entropy production. In the resulting general constitutive model, the key ingredients for the material modeling is the free energy density which defines the equilibrium properties of the system.

Balance equations. The electric field \mathbf{E} , the barycentric velocity \mathbf{v} and the number densities n_α for $\alpha \in \mathcal{I}$ are determined from the Poisson equation and the balance equations of momentum and partial mass, viz.

$$\text{curl}(\mathbf{E}) = 0 , \quad (2.4a)$$

$$\text{div}(\varepsilon_0 \mathbf{E} + \mathbf{P}) = q , \quad (2.4b)$$

$$\partial_t(\rho \mathbf{v}) + \text{div}(\rho \mathbf{v} \otimes \mathbf{v} - \boldsymbol{\sigma}) = q \mathbf{E} + (\nabla \mathbf{E}) \mathbf{P} , \quad (2.4c)$$

$$\partial_t n_\alpha + \text{div}(n_\alpha \mathbf{v} + \mathbf{J}_\alpha) = \sum_{m=1}^M \nu_{\alpha,m} r_m \quad \text{for } \alpha \in \mathcal{I} . \quad (2.4d)$$

Here the – yet undetermined– constitutive quantities are the vector of polarization \mathbf{P} , the symmetric (Cauchy) stress tensor $\boldsymbol{\sigma}$, and the diffusional fluxes \mathbf{J}_α with the constraint $\sum_{\alpha \in \mathcal{I}} m_\alpha \mathbf{J}_\alpha = 0$ and the reaction rates r_m .

As long, as $\boldsymbol{\sigma}$ is not specified, there is no unique way to write the momentum balance, since terms can freely be moved from the stresses to the forces and back. This is discussed in more detail in Sect. 3.2 below. However, in order to remove all ambiguity, we introduce the total stress tensor $\boldsymbol{\Sigma}$, viz.

$$\boldsymbol{\Sigma} = \boldsymbol{\sigma} + (\varepsilon_0 \mathbf{E} + \mathbf{P}) \otimes \mathbf{E} - \frac{1}{2}(\varepsilon_0 \mathbf{E} \cdot \mathbf{E}) \mathbf{1} , \quad (2.5)$$

whereby we can rewrite the momentum balance as

$$\partial_t(\rho \mathbf{v}) + \operatorname{div}(\rho \mathbf{v} \otimes \mathbf{v} - \boldsymbol{\Sigma}) = 0 . \quad (2.6)$$

Constitutive equations. The constitutive equations or material functions of our model framework are derived exclusively from a free energy density $\rho\xi$, for which we assume the rather general structure

$$\rho\xi = \rho\xi(T, (n)_{\alpha \in \mathcal{I}}, \mathbf{P}) . \quad (2.7)$$

We introduce the chemical potentials and the equilibrium electric field as

$$\mu_\alpha := \frac{\partial \rho\xi}{\partial n_\alpha} \quad \text{for } \alpha \in \mathcal{I} , \quad \mathbf{E}^{\text{Eq}} := \frac{\partial \rho\xi}{\partial \mathbf{P}} , \quad (2.8)$$

which depend on $(T, (n)_{\alpha \in \mathcal{I}}, \mathbf{P})$. Application of the entropy principle [20] yields for the reaction rates r_m , the (diffusion) fluxes \mathbf{J}_α , the polarization \mathbf{P} , and the stress tensor $\boldsymbol{\sigma}$, the relations

$$r_m = L_m \cdot \left(e^{\frac{\lambda'_m}{k_B T}} - e^{-\frac{\lambda''_m}{k_B T}} \right) \quad \text{with } \lambda'_m := \sum_{\alpha \in \mathcal{I}} \nu'_{\alpha, m} \mu_\alpha \quad \text{and } \lambda''_m := \sum_{\alpha \in \mathcal{I}} \nu''_{\alpha, m} \mu_\alpha , \quad (2.9a)$$

$$\mathbf{J}_\alpha = - \sum_{\beta \in \mathcal{I} \setminus 0} M_{\alpha\beta} \cdot \left(\nabla \mu_\beta - \frac{m_\beta}{m_0} \nabla \mu_0 + z_\beta e_0 \mathbf{E} \right) \quad \text{for } \alpha \in \mathcal{I} \setminus 0 , \quad (2.9b)$$

$$\partial_t \mathbf{P} = \frac{\varepsilon_0}{\tau_P} \cdot (\mathbf{E} - \mathbf{E}^{\text{Eq}}) - (\mathbf{v} \cdot \nabla) \mathbf{P} , \quad (2.9c)$$

$$\boldsymbol{\sigma} = \left(\rho\xi - \sum_{\alpha \in \mathcal{I}} n_\alpha \mu_\alpha - \mathbf{E}^{\text{Eq}} \cdot \mathbf{P} \right) \mathbf{1} + \boldsymbol{\sigma}^{\text{visc}} + \boldsymbol{\sigma}^{\text{pol}} \quad \text{with} \quad (2.9d)$$

$$\boldsymbol{\sigma}^{\text{visc}} = \nu_s \operatorname{div}(\mathbf{v}) \mathbf{1} + \nu_b (\nabla \mathbf{v} + (\nabla \mathbf{v})^T) , \quad (2.9e)$$

$$\boldsymbol{\sigma}^{\text{pol}} = ((\mathbf{E}^{\text{Eq}} - \mathbf{E}) \cdot \mathbf{P}) \mathbf{1} . \quad (2.9f)$$

The phenomenological coefficients can be arbitrary functions of the independent variables, such that the reaction rate constants $L_m > 0$, $M_{\alpha\beta}$ defines a positive definite matrix, the polarization relaxation time $\tau_P > 0$, and bulk and shear viscosity $(\nu_s + \frac{2}{3}\nu_b) > 0$ and $\nu_b > 0$.

Pressure. The pressure within the system is introduced via

$$p =: -\frac{1}{3} \operatorname{tr}(\boldsymbol{\sigma} - \boldsymbol{\sigma}^{\text{visc}} - \boldsymbol{\sigma}^{\text{pol}}) , \quad (2.10)$$

such that p satisfies the Gibbs-Duhem equation

$$p = -\rho\xi + \sum_{\alpha \in \mathcal{I}} n_\alpha \mu_\alpha + \mathbf{E}^{\text{Eq}} \cdot \mathbf{P} . \quad (2.11)$$

This implies in polarizable media

$$\nabla p = \sum_{\alpha \in \mathcal{I}} n_\alpha \nabla \mu_\alpha + (\nabla \mathbf{E}^{\text{Eq}}) \mathbf{P} . \quad (2.12)$$

Equilibrium. In the following we consider thermodynamic equilibrium of the various dissipative processes. This implies

- Chemical reaction equilibrium: vanishing affinity $\lambda_m =: \lambda_m'' - \lambda_m'$ implies

$$0 = \sum_{\alpha \in \mathcal{I}} \nu_{\alpha,m} \mu_\alpha \quad m = 1, \dots, M. \quad (2.13a)$$

- Diffusional equilibrium $0 = \mathbf{J}_\alpha$, such that a positive definite mobility matrix implies

$$0 = \nabla \left(\mu_\alpha - \frac{m_\alpha}{m_0} \mu_0 \right) + z_\alpha e_0 \mathbf{E} \quad \text{for } \alpha \in \mathcal{I} \setminus 0. \quad (2.13b)$$

- Polarization vector equilibrium:

$$\mathbf{E} = \mathbf{E}^{\text{Eq}}, \quad (2.13c)$$

- Mechanical equilibrium $0 = \boldsymbol{\sigma}^{\text{visc}}$, (2.4c) implies

$$\nabla p = q \mathbf{E} + (\nabla \mathbf{E}) \mathbf{P}. \quad (2.13d)$$

Debye relaxation. The evolution equation (2.9c), where \mathbf{E}^{Eq} is a general function of the variables $(T, (n)_{\alpha \in \mathcal{I}}, \mathbf{P})$, is essentially a generalization of the Debye relaxation equation. For a vanishing barycentric velocity, i.e. $\mathbf{v} = 0$, and a simple polarization model $\mathbf{E}^{\text{Eq}} = \frac{1}{\chi \varepsilon_0} \mathbf{P}$, with $\chi = \text{const.}$, the Debye relaxation is obtained from (2.9c), i.e.

$$\chi \tau_P \partial_t \mathbf{P} + \mathbf{P} = \varepsilon_0 \chi \mathbf{E}. \quad (2.14)$$

Denoting with $\hat{\mathbf{P}}(\cdot, \omega) = \mathcal{F}(\mathbf{P}(\cdot, t))$ the Fourier transformed polarization (and $\hat{\mathbf{E}}$ accordingly), (2.14) yields

$$\chi \tau_P i \omega \hat{\mathbf{P}} + \hat{\mathbf{P}} = \chi \varepsilon_0 \hat{\mathbf{E}} \quad (2.15)$$

and thus

$$\hat{\mathbf{P}} = \varepsilon_0 (\hat{\chi}' - i \hat{\chi}'') \hat{\mathbf{E}} \quad (2.16)$$

with

$$\hat{\chi}' := \frac{\chi}{1 + \left(\frac{\omega}{\omega_0}\right)^2}, \quad \hat{\chi}'' := \frac{\chi \frac{\omega}{\omega_0}}{1 + \left(\frac{\omega}{\omega_0}\right)^2} \quad \text{and} \quad \omega_0 := \frac{1}{\chi \tau_P}. \quad (2.17)$$

For the electric displacement field $\mathbf{D} := \varepsilon_0 \mathbf{E} + \mathbf{P}$ we obtain hence

$$\hat{\mathbf{D}} = (\hat{\varepsilon}'_r - i \hat{\varepsilon}''_r) \varepsilon_0 \hat{\mathbf{E}} \quad (2.18)$$

with

$$\hat{\varepsilon}'_r := 1 + \chi' \quad \text{and} \quad \hat{\varepsilon}''_r = \hat{\chi}'', \quad (2.19)$$

which corresponds to the classical decomposition of the Fourier transformed relative dielectric $\hat{\varepsilon}_r$. We emphasize, however, that for more complex dependencies of \mathbf{E}^{Eq} on $(T, (n)_{\alpha \in \mathcal{I}}, \mathbf{P})$, such decompositions can in general not be obtained and that the polarization evolution remains coupled to the species balance equations (2.4d).

Extended diffusional equilibrium. From the equilibrium conditions (2.13b), we get

$$\sum_{\alpha \in \mathcal{I}} n_{\alpha} \nabla \mu_{\alpha} = q \mathbf{E} + \frac{\rho}{m_0} \nabla \mu_0 . \quad (2.20)$$

Inserting (2.13c) into (2.12) yields

$$\nabla p = \sum_{\alpha \in \mathcal{I}} n_{\alpha} \nabla \mu_{\alpha} + (\nabla \mathbf{E}) \mathbf{P} . \quad (2.21)$$

Thus, combining (2.21) and (2.20) with (2.13d) we can first conclude that $\nabla \mu_0 = 0$. In a next step, using the electrostatic potential φ such that $\mathbf{E} = -\nabla \varphi$, we obtain for the electrochemical potential $\mu_{\alpha} + e_0 z_{\alpha} \varphi$ of all species the well known equilibrium conditions

$$\nabla(\mu_{\alpha} + e_0 z_{\alpha} \varphi) = 0 \quad \text{for all } \alpha \in \mathcal{I} . \quad (2.22)$$

We emphasize, that this is a consequence from the consistent coupling of the diffusional equilibrium with the momentum balance and the mechanical and polarization equilibrium. Therefore, we call the conditions (2.22) *extended diffusional equilibrium* in the following.

2.3 Material model for the electrolyte with concentration dependent susceptibility

In this section we state explicit functions for the free energy density, and subsequently for the chemical potential as well as the polarization vector. Aim of this section is not to rigorously derive the functions, based on some microscopic theory, but rather discuss their thermodynamic consequences. In the above application of the entropy principle we followed the approach of [20] based on the entropy as a constitutive function of the vector of polarization \mathbf{P} , in order to obtain a stable relaxation to equilibrium with the Debye equation (2.9c). However, for the formulation of constitutive laws, it seems more naturally to describe the free energy density in terms of the (equilibrium) electric field \mathbf{E}^{Eq} . Therefore we first apply a change of variables.

Legendre transformation for $\rho \xi$. We consider the Legendre transformation $\rho \psi := \rho \xi - \mathbf{P} \cdot \mathbf{E}^{\text{Eq}}$. By definition we then have

$$\frac{\partial \rho \psi}{\partial \mathbf{E}^{\text{Eq}}} = -\mathbf{P} \quad \text{and} \quad \rho \psi = \rho \psi(T, (n_{\alpha})_{\alpha \in \mathcal{I}}, \mathbf{E}^{\text{Eq}}) , \quad (2.23)$$

and obtain thus the Gibbs-Duhem equation

$$p = -\rho \psi + \sum_{\alpha \in \mathcal{I}} n_{\alpha} \mu_{\alpha} . \quad (2.24)$$

From this perspective, one might term $\rho \psi$ also the free energy density of the mixture, however in the variables $(T, (n_{\alpha})_{\alpha \in \mathcal{I}}, \mathbf{E}^{\text{Eq}})$. For the chemical potential as defined by (2.8), we obtain

$$\mu_{\alpha} = \frac{\partial \rho \psi((n_{\beta})_{\beta \in \mathcal{I}}, \mathbf{E}^{\text{Eq}})}{\partial n_{\alpha}} . \quad (2.25)$$

In the following, we drop the superscript $^{\text{Eq}}$ of \mathbf{E}^{Eq} in the functional dependency of $\rho \psi$ for the sake of a compact typeface, but emphasize again that in the non-equilibrium case \mathbf{E}^{Eq} and \mathbf{E} remain different.

In the following we skip the super-script $^{\text{Eq}}$ to simplify notation.

Free energy density. We consider a free energy density that are a superposition of several contributions, i.e. we introduce

$$\rho\psi = \sum_k \rho\psi^k, \quad \mu_\alpha^k = \frac{\partial \rho\psi^k}{\partial n_\alpha}, \quad p^k = -\rho\psi^k + \sum_\alpha n_\alpha \mu_\alpha^k. \quad (2.26)$$

Since we are interested in obtaining only material functions for \mathbf{P} with a scalar susceptibility χ , we restrict the constitutive function for the free energy to the structure

$$\rho\psi = \rho\psi^{\text{mat}}((n_\alpha)_{\alpha \in \mathcal{I}}) + \rho\psi^{\text{pol}}((n_\alpha)_{\alpha \in \mathcal{I}}, \mathbf{E}), \quad (2.27)$$

such that $\mu_\alpha = \mu_\alpha^{\text{mat}} + \mu_\alpha^{\text{pol}}$ and $p = p^{\text{mat}} + p^{\text{pol}}$.

The material model for $\rho\psi^{\text{mat}}$ describes the electrolyte as an incompressible mixture of solvated ions and we refer to [19, 34] for a detailed derivation and analysis of $\rho\psi^{\text{mat}}$. The resulting expressions for the thermodynamic potentials are

$$\mu_\alpha^{\text{mat}} = \psi_\alpha^{\text{E}} + k_B T \ln(y_\alpha) + v_\alpha^{\text{E}} p^{\text{mat}} \quad \text{for } \alpha \in \mathcal{I}, \quad \text{with } y_\alpha = \frac{n_\alpha}{\sum_{\beta \in \mathcal{I}} n_\beta}, \quad (2.28)$$

where ψ_α^{E} is the free energy density of the constituent A_α of a reference configuration in the electrolyte [34]. In this model, incompressibility is obtained as the limiting case for large isotropic bulk modulus. As a consequence, we have an algebraic constraint

$$\sum_{\alpha \in \mathcal{I}} v_\alpha^{\text{E}} n_\alpha = 1. \quad (2.29)$$

Since μ_α^{mat} is expressed in terms of p^{mat} , we rewrite the momentum balance as

$$\nabla p^{\text{mat}} = q \mathbf{E} + (\nabla \mathbf{E}) \mathbf{P} - \nabla p^{\text{pol}}. \quad (2.30)$$

and emphasize again that $p^{\text{pol}} = -\rho\psi^{\text{pol}} + \sum_\alpha n_\alpha \mu_\alpha^{\text{pol}}$.

For the polarization contribution $\rho\psi^{\text{pol}}$ we consider only free energy functions which yield the representation

$$\frac{\partial \rho\psi^{\text{pol}}}{\partial \mathbf{E}} = -\mathbf{P} \quad \text{and} \quad \mathbf{P} = \varepsilon_0 \chi((n_\alpha)_{\alpha \in \mathcal{I}}, \mathbf{E}) \mathbf{E}. \quad (2.31)$$

Note that there is a practical representation of $\rho\psi^{\text{pol}}$ when $|\mathbf{E}|^2$ is considered as variable as well as $\chi((n_\alpha)_{\alpha \in \mathcal{I}}, \mathbf{E}) = \hat{\chi}((n_\alpha)_{\alpha \in \mathcal{I}}, |\mathbf{E}|^2)$, i.e.

$$\rho\psi^{\text{pol}} = - \int_0^{\mathbf{E}} \varepsilon_0 \chi(n_\alpha, \mathbf{E}') \mathbf{E}' d\mathbf{E}' = -\frac{1}{2} \varepsilon_0 \int_0^{|\mathbf{E}|^2} \varepsilon_0 \hat{\chi}(n_\alpha, \mathbf{F}) d\mathbf{F} = -\frac{\varepsilon_0}{2} X(n_\alpha, |\mathbf{E}|^2) \quad (2.32)$$

$$\text{with } X(n_\alpha, |\mathbf{E}|^2) := \int_0^{|\mathbf{E}|^2} \varepsilon_0 \hat{\chi}(n_\alpha, \zeta) d\zeta \quad \text{and} \quad \frac{\partial X}{\partial |\mathbf{E}|^2} = \hat{\chi}(n_\alpha, |\mathbf{E}|^2). \quad (2.33)$$

Hence we can write

$$\mu_\alpha^{\text{pol}} = -\frac{\varepsilon_0}{2} \frac{\partial X}{\partial n_\alpha} \quad \text{and} \quad p^{\text{pol}} = \frac{\varepsilon_0}{2} \left(X(n_\alpha, |\mathbf{E}|^2) - \sum_{\alpha \in \mathcal{I}} n_\alpha \frac{\partial X}{\partial n_\alpha} \right). \quad (2.34)$$

For a further classification of material functions χ , we consider the following cases:

(Case 0): Constant susceptibility

$$\chi = \hat{\chi}^{(0)} = \text{const.} \quad (2.35)$$

This is obtained by $\rho\psi^{\text{pol}} = -\chi_0 \frac{\varepsilon_0}{2} |\mathbf{E}|^2$ and implies

$$\mu_\alpha^{\text{pol}} = 0 \quad \text{for } \alpha \in \mathcal{I}, \quad p^{\text{pol}} = -\rho\psi^{\text{pol}}. \quad (2.36a)$$

The momentum balance reduces to

$$\nabla p^{\text{mat}} = q \mathbf{E} + (\nabla \mathbf{E}) \mathbf{P} + \nabla(\rho\psi^{\text{pol}}) = q \mathbf{E} \quad (2.36b)$$

since $\nabla \rho\psi^{\text{pol}} = -\mathbf{P}(\nabla \mathbf{E})$ and the Poisson equation reads

$$\text{div}((1 + \hat{\chi}^{(0)})\varepsilon_0 \mathbf{E}) = q. \quad (2.36c)$$

(Case 1): Electric field dependent susceptibility

$$\chi = \hat{\chi}^{(1)}(|\mathbf{E}|^2). \quad (2.37)$$

This is obtained by $\rho\psi^{\text{pol}} = -\frac{\varepsilon_0}{2} X(|\mathbf{E}|^2)$ with $\hat{\chi}^{(1)}(|\mathbf{E}|^2) = \frac{\partial X}{\partial |\mathbf{E}|^2}$ and implies as in (Case 0)

$$\mu_\alpha^{\text{pol}} = 0 \quad \text{for } \alpha \in \mathcal{I}, \quad p^{\text{pol}} = -\rho\psi^{\text{pol}}. \quad (2.38a)$$

The momentum balance reduces to

$$\nabla p^{\text{mat}} = q \mathbf{E} + (\nabla \mathbf{E}) \mathbf{P} + \nabla(\rho\psi^{\text{pol}}) = q \mathbf{E} \quad (2.38b)$$

since $\nabla \rho\psi^{\text{pol}} = -\mathbf{P}(\nabla \mathbf{E})$ and the Poisson equation reads

$$\text{div}((1 + \hat{\chi}(|\mathbf{E}|^2))\varepsilon_0 \mathbf{E}) = q. \quad (2.38c)$$

(Case 2): Concentration dependent susceptibility

$$\chi = \sum_{\alpha \in \mathcal{I}} v_\alpha^{\text{E}} n_\alpha \cdot \chi_\alpha =: \hat{\chi}^{(2)}((n_\alpha)_{\alpha \in \mathcal{I}}), \quad (2.39)$$

with constant χ_α for $\alpha \in \mathcal{I}$. This is obtained by $\rho\psi^{\text{pol}} = -\sum_{\alpha \in \mathcal{I}} v_\alpha^{\text{E}} n_\alpha \cdot \chi_\alpha \frac{\varepsilon_0}{2} |\mathbf{E}|^2$, which is homogeneous of degree one with respect to the number densities n_α and implies

$$\mu_\alpha^{\text{pol}} = -v_\alpha^{\text{E}} \cdot \chi_\alpha \frac{\varepsilon_0}{2} |\mathbf{E}|^2 \quad \text{for } \alpha \in \mathcal{I}, \quad p^{\text{pol}} = 0. \quad (2.40a)$$

The momentum balance reduces to

$$\nabla p^{\text{mat}} = q \mathbf{E} + \chi^{(2)}((n_\alpha)_{\alpha \in \mathcal{I}}) (\nabla \mathbf{E}) \cdot \varepsilon_0 \mathbf{E} \quad (2.40b)$$

and the Poisson equation reads

$$\text{div}((1 + \hat{\chi}^{(2)}((n_\alpha)_{\alpha \in \mathcal{I}}))\varepsilon_0 \mathbf{E}) = q. \quad (2.40c)$$

(Case 3): Concentration and electric field dependent susceptibility

$$\chi = \sum_{\alpha \in \mathcal{I}} v_{\alpha}^{\mathbf{E}} n_{\alpha} \cdot \chi_{\alpha}(|\mathbf{E}|^2) =: \hat{\chi}^{(3)}((n_{\alpha})_{\alpha}, |\mathbf{E}|^2) \quad (2.41)$$

This is obtained by $\rho\psi^{\text{pol}} = -\sum_{\alpha \in \mathcal{I}} v_{\alpha}^{\mathbf{E}} n_{\alpha} \cdot \frac{\varepsilon_0}{2} X_{\alpha}(|\mathbf{E}|^2)$ with $\chi_{\alpha}(|\mathbf{E}|^2) = \frac{\partial X_{\alpha}}{\partial |\mathbf{E}|^2}$ and implies analogously to (Case 2)

$$\mu_{\alpha}^{\text{pol}} = -v_{\alpha}^{\mathbf{E}} \cdot \frac{\varepsilon_0}{2} X_{\alpha}(|\mathbf{E}|^2) \quad \text{for } \alpha \in \mathcal{I}, \quad p^{\text{pol}} = 0. \quad (2.42a)$$

The momentum balance reduces to

$$\nabla p^{\text{mat}} = q \mathbf{E} + \hat{\chi}^{(3)}((n_{\alpha})_{\alpha}, |\mathbf{E}|^2) (\nabla \mathbf{E}) \cdot \varepsilon_0 \mathbf{E} \quad (2.42b)$$

and the Poisson equation reads

$$\text{div} \left((1 + \hat{\chi}^{(3)}((n_{\alpha})_{\alpha \in \mathcal{I}}, |\mathbf{E}|^2)) \varepsilon_0 \mathbf{E} \right) = q. \quad (2.42c)$$

Typical examples for $\rho\psi^{\text{pol}}$ and χ in the (Case 1) are

$$\rho\psi^{\text{pol}} = -\frac{\varepsilon_0}{a} \chi_0 \sqrt{1 + a|\mathbf{E}|^2}, \quad \mathbf{P} = \frac{\chi_S}{\sqrt{1 + a|\mathbf{E}|^2}} \cdot \varepsilon_0 \mathbf{E}, \quad (2.43a)$$

$$\rho\psi^{\text{pol}} = -\frac{3\varepsilon_0}{a} \chi_0 \ln \left(\frac{\sinh(\sqrt{a}|\mathbf{E}|)}{\sqrt{a}|\mathbf{E}|} \right), \quad \mathbf{P} = \frac{3\chi_S}{\sqrt{a}|\mathbf{E}|} L(\sqrt{a}|\mathbf{E}|) \cdot \varepsilon_0 \mathbf{E}, \quad (2.43b)$$

with the Langevin function $L(x) = \coth(x) - \frac{1}{x}$. While (2.43b) is related to the theory of [15, 43, 9], (2.43a) follows the more pragmatic choice of [27, (eqn. 17)]. We note that (2.43a) corresponds to the case $m = 1/2$ of the general approach

$$\rho\psi^{\text{pol}} = -\frac{\varepsilon_0}{a} \frac{m}{1-m} \chi_0 \left(1 + \frac{a}{2m} |\mathbf{E}|^2\right)^{1-m}, \quad \mathbf{P} = \chi_0 \left(1 + \frac{a}{2m} |\mathbf{E}|^2\right)^{-m} \cdot \varepsilon_0 \mathbf{E} \quad (2.44)$$

proposed in [27], where further on $0 < m < 2$ is conjectured. However, considering the one-dimensional case, the Poisson equation is

$$-\varepsilon_0 \left(1 + \chi(|\partial_x \varphi|) + \chi'(|\partial_x \varphi|) \partial_x \varphi\right) \partial_{xx} \varphi = q \quad (2.45)$$

For the given examples, we check

$$\chi + \chi'(|\partial_x \varphi|) \partial_x \varphi = \chi_S \cdot \begin{cases} \frac{1}{\sqrt{1+a|\partial_x \varphi|^2}^3} & \text{in case of (2.43a)}, \\ 3L'(\sqrt{a}|\partial_x \varphi|) & \text{in case of (2.43b)}, \\ \frac{1-a\frac{2m-1}{2m}|\partial_x \varphi|^2}{(1+a|\partial_x \varphi|^2)^2} & \text{in case of (2.44)}, \end{cases} \quad (2.46)$$

Thus, we conclude that $\chi + \chi' \partial_x \varphi > 0$ for (2.43b) and (2.43a), whereas (2.44) with $m > 1/2$, violates the ellipticity condition if $|\mathbf{E}|$ is sufficiently large.

Extended diffusion equilibrium. The constant electrochemical potentials according to (2.22) yield at any point x in space the identity

$$\begin{aligned} y_\alpha(x) &= y_\alpha^{\text{bulk}} \cdot \exp\left(-\frac{e_0 z_\alpha}{k_B T}(\varphi(x) - \varphi^{\text{bulk}}) - \frac{v_\alpha^E}{k_B T}(p^{\text{mat}}(x) - p^{\text{bulk}}) + \frac{1}{k_B T}(\mu_\alpha^{\text{pol}}(|\mathbf{E}(x)|) - \mu_\alpha^{\text{pol}}(|\mathbf{E}^{\text{bulk}}|))\right) \\ &= \hat{y}_\alpha(\varphi, p^{\text{mat}}, |\mathbf{E}|). \end{aligned} \quad (2.47)$$

where $y_\alpha^{\text{bulk}}, p^{\text{bulk}}, \varphi^{\text{bulk}}$ denote the corresponding bulk quantities. Therefore, we conclude the existence of representations

$$y_\alpha = \begin{cases} \hat{y}_\alpha^{(k)}(\varphi, p^{\text{mat}}) & \text{if } k = 0, 1, \\ \hat{y}_\alpha^{(k)}(\varphi, p^{\text{mat}}, |\mathbf{E}|) & \text{if } k = 2, 3, \end{cases} \quad (2.48)$$

from (2.36a), (2.38a), (2.40a), (2.42a), respectively. The incompressibility constraint (2.29) yields the relations

$$n_\alpha = \frac{y_\alpha}{\sum_{\beta \in \mathcal{I}} v_\beta^E y_\beta}, \quad q = e_0 \frac{\sum_{\alpha \in \mathcal{I}} z_\alpha y_\alpha}{\sum_{\alpha \in \mathcal{I}} v_\alpha^E y_\alpha}, \quad \text{and } \hat{\chi}^{(k)} = \frac{\sum_{\alpha \in \mathcal{I}} v_\alpha^E y_\alpha \chi_\alpha}{\sum_{\alpha \in \mathcal{I}} v_\alpha^E y_\alpha}, \quad k = 2, 3. \quad (2.49)$$

Thus, we obtain further representations in terms of the variables $(\varphi, p^{\text{mat}}, |\mathbf{E}|)$ for (Case k), viz.

$$n_\alpha = \begin{cases} \hat{n}_\alpha^{(k)}(\varphi, p^{\text{mat}}) & \text{if } k = 0, 1, \\ \hat{n}_\alpha^{(k)}(\varphi, p^{\text{mat}}, |\mathbf{E}|) & \text{if } k = 2, 3, \end{cases} \quad q = \begin{cases} \hat{q}^{(k)}(\varphi, p^{\text{mat}}) & \text{if } k = 0, 1, \\ \hat{q}^{(k)}(\varphi, p^{\text{mat}}, |\mathbf{E}|) & \text{if } k = 2, 3, \end{cases} \quad (2.50)$$

$$\text{and } \chi = \begin{cases} \hat{\chi}^{(0)} & \text{if } k = 0, \\ \hat{\chi}^{(1)}(|\mathbf{E}|) & \text{if } k = 1, \\ \hat{\chi}^{(k)}(\varphi, p^{\text{mat}}, |\mathbf{E}|) & \text{if } k = 2, 3. \end{cases} \quad (2.51)$$

In summary, the state of the electrolyte is determined in the extended diffusion equilibrium by the Poisson equation (2.36c), (2.38c), (2.40c), or (2.42c), respectively, and the corresponding momentum balance (2.36b), (2.42b), (2.40b), or (2.38b). Note that the constraint $\sum_{\alpha \in \mathcal{I}} y_\alpha = 1$ for the mole fractions y_α , which holds for every point x in space and for every material model, can either be used to express the solvent mole fraction in terms of the ionic species or to substitute the momentum balance by an algebraic constraint, yielding the differential algebraic equation system ($k = 0, 1, 2, 3$)

$$\text{div}((1 + \hat{\chi}^{(k)})\varepsilon_0 \nabla \varphi) = \hat{q}^{(k)}, \quad (2.52a)$$

$$\sum_{\alpha \in \mathcal{I}} \hat{y}_\alpha^{(k)} = 1. \quad (2.52b)$$

2.4 Interface of a planar metal electrode and the electrolyte

Our main discussion of section 3 and 4 is based on an experimental three electrode setup [34] which allows to investigate the interface between a planar (single crystal) electrode and the adjacent electrolyte for an applied voltage between these two phases. Therewith we can compute (i) the space charge layer structure (ii) the charge stored in the whole space charge layer and (iii) the corresponding differential capacity in terms of the applied voltage.

We consider in the following a 1D-approximation of a planar metal electrode, where the electrode surface is located at $x = 0$ and the bulk electrolyte at $x = x^{\text{bulk}}$ and denote with $u^{\text{surf}} := u(x = 0)$ and $u^{\text{bulk}} := u(x^{\text{bulk}})$ for some space dependent function $u(x)$. Throughout this work we consider

exclusively non-adsorbing electrolytes, but emphasize that specific adsorption can be consistently taken into account and we refer to [34, 18] for details.

We consider a surprisingly simple material function for the surface chemical potential of electrons such that μ_e is constant with respect to the number density of surface electrons $n_{e,s}$. The constant is related to the work function of the specific metal surface in order to account for different surface orientations. This material model ensures, in accordance with Kohn-Sham-theory, that excess electrons are exclusively stored on the metal surface and that the potential drop in the metal boundary layer remains constant (w.r.t. applied voltage).

Boundary conditions. In a three electrode setup, it is possible to derive

$$\varphi|_{x=0} - \varphi^{\text{bulk}} = U^{\text{Meas}} - U^{\text{ref}} =: U \quad (2.53)$$

where U^{ref} depends on the work function of the specific metal surface as well as the reference electrode and we refer to [34] for details on the derivation. U is the actual potential drop across the electrolytic space charge layer and U^{Meas} the measured voltage in a three electrode setup.

The electric field $E = -\partial_x \varphi$ field is supposed to vanish in the bulk, *i.e.* $E^{\text{bulk}} = 0$.

Dissociation reaction equilibrium. For an electrolyte which consist only of a solvent S , anions A , cations C and ion pairs AC , the relation (2.13a) for the thermodynamic equilibrium of the dissociation reaction (2.2), *i.e.*

$$\mu_{AC} + (\kappa_A + \kappa_C)\mu_S = \mu_A + \mu_C, \quad (2.54)$$

yields a constraint to determine the concentration of the ion pair AC . We assume that the volume and the mass are conserved during the dissociation reaction, which entails

$$v_A^E + v_C^E = v_{AC}^E + (\kappa_A + \kappa_C)v_S^E \quad \text{and} \quad m_A + m_C = (\kappa_A + \kappa_C)m_S + m_{AC}. \quad (2.55)$$

Introducing the dissociation degree δ via $n_A^{\text{bulk}} = n_C^{\text{bulk}} = \delta \cdot c$ and $n_{AC}^{\text{bulk}} = (1 - \delta)c$, where c is the prescribed salt concentration, yields the constraint

$$f(c, \delta) =: e^{-\frac{\Delta g}{k_B T}} - \frac{\delta^2 \cdot c}{(1 - \delta)} \cdot \frac{v_S}{(1 + (2v_S - (v_A + v_C))\delta c + (v_S - v_{AC})\delta(1 - c))} \cdot \left(\frac{(1 - (v_A + v_C)\delta c - v_{AC}\delta(1 - c))}{1 + (v_S^2 - (v_A + v_C))\delta c + (v_S - v_{AC})\delta(1 - c)} \right)^{-(\kappa_A + \kappa_C)} \stackrel{!}{=} 0 \quad (2.56)$$

with

$$\Delta g = \psi_A^E + \psi_C^E - \psi_{AC}^E - (\kappa_A + \kappa_C)\psi_S^E, \quad (2.57)$$

which is actually a generalization of Ostwald's dilution law when solvation effects are considered [33]. This relation can be used to deduce from $f(\delta, c) = 0$ a (local) expression $\delta = \hat{\delta}(c)$ for the dissociation degree.

Extended diffusion equilibrium. The Poisson equation(2.4b) and the momentum balance (2.13d) for the cases $k = 0, 1, 2, 3$ with the representations (2.50) of q essentially read

(Case 0 and 1):

$$E = -\partial_x \varphi \quad (2.58a)$$

$$\partial_x (\varepsilon_0 (1 + \hat{\chi}^{(k)}(|E|)) \cdot E) = \hat{q}(\varphi, p^{\text{mat}}) \quad (2.58b)$$

$$\partial_x p^{\text{mat}} = \hat{q}(\varphi, p^{\text{mat}}) \cdot E \quad (2.58c)$$

(Case 2 and 3):

$$E = -\partial_x \varphi \quad (2.59a)$$

$$\partial_x (\varepsilon_0 (1 + \hat{\chi}^{(k)}(\varphi, p^{\text{mat}}, |E|)) \cdot E) = \hat{q}(\varphi, p^{\text{mat}}, |E|) \quad (2.59b)$$

$$\partial_x p^{\text{mat}} = \hat{q}(\varphi, p^{\text{mat}}, |E|) \cdot E + \varepsilon_0 \hat{\chi}^{(k)}(\varphi, p^{\text{mat}}, |E|) \cdot (\partial_x E) E \quad (2.59c)$$

We emphasize that that our derived Poisson-Momentum balance equation system (2.58a)–(2.58c) is a highly non-linear coupled ODE system, in contrast to common Poisson–Boltzmann approaches and various extensions, as we discuss in more detail in Sect. 3.1.

Electric field-pressure relation and boundary layer charge. In the case of a planar one-dimensional setting, the stationary electric field is given as $E = -\partial_x \varphi$ and the x -component of the total stress tensor Σ reduces to

$$\Sigma = -p^{\text{mat}} - p^{\text{pol}} + \varepsilon_0 (1 + \chi) |E|^2 - \frac{\varepsilon_0}{2} |E|^2. \quad (2.60)$$

The momentum balance (2.6) implies the constancy of the total stress, whereby at each point $x \geq 0$ in the electrolyte domain it holds

$$p^{\text{mat}} - p^{\text{bulk}} = \varepsilon_0 (1 + \chi) |E|^2 - \frac{\varepsilon_0}{2} |E|^2 - p^{\text{pol}}, \quad (2.61)$$

$p^{\text{pol}} = 0$ for Case 2 and 3. Thus, we have

$$p^{\text{mat}} - p^{\text{bulk}} = \begin{cases} \frac{\varepsilon_0}{2} (1 + \chi) |E|^2 & \text{for Case 0 ,} \\ \frac{\varepsilon_0}{2} (1 + \chi) |E|^2 + (\rho \psi^{\text{pol}}(|E|) + \frac{\varepsilon_0}{2} \chi |E|^2) & \text{for Case 1 ,} \\ \frac{\varepsilon_0}{2} (1 + 2\chi) |E|^2 & \text{for Case 2 and 3 .} \end{cases} \quad (2.62)$$

Given a value of $\varphi - \varphi^{\text{bulk}}$, (2.62) together with the constraint $\sum_{\alpha \in \mathcal{I}} y_\alpha = 1$ from the definition (2.28) and using the representations (2.50) defines an a system of two algebraic relation that determine $p^{\text{mat}} = \check{p}^{\text{mat}}(\varphi - \varphi^{\text{bulk}})$ and $E = \check{E}(\varphi - \varphi^{\text{bulk}})$. Using the representations (2.50), then $\chi = \check{\chi}(\varphi - \varphi^{\text{bulk}})$ can be deduced. However, for given values of φ it is possible to determine p^{mat} and E from the nonlinear algebraic equation system

$$\vec{g}(\varphi, p^{\text{mat}}, E) = \vec{0} \quad \text{with} \quad \vec{g} = (g_1, g_2) \quad (2.63)$$

$$\text{and } g_1 := 1 - \sum_{\alpha} y_{\alpha}, \quad g_2 := p^{\text{mat}} - p^{\text{bulk}} - \varepsilon_0 (1 + \chi) |E|^2 + \frac{\varepsilon_0}{2} |E|^2 + p^{\text{pol}} \quad (2.64)$$

as (local solutions) $p^{\text{mat}} = \check{p}^{\text{mat}}(\varphi)$, $E = \check{E}(\varphi)$ via the implicit function theorem. Note that

$$g_1 = \begin{cases} g_1^{(k)}(\varphi, p, E), & \text{if } k = 0, 1 \\ g_1^{(k)}(\varphi, p^{\text{mat}}, E) & \text{if } k = 2, 3 \end{cases} \quad \text{and} \quad g_2 = \begin{cases} g_2^{(k)}(p^{\text{mat}}, E), & \text{if } k = 0, 1 \\ g_2^{(k)}(\varphi, p^{\text{mat}}, E), & \text{if } k = 2, 3 \end{cases}. \quad (2.65)$$

These relations can be used to determine the boundary layer charge

$$Q = - \int_0^{x^{\text{bulk}}} q dx = \left(\varepsilon_0 (1 + \chi) \cdot E \right) \Big|_{x=0} \quad (2.66)$$

as function of the potential difference $U = \varphi|_{x=0} - \varphi^{\text{bulk}}$ from (2.62) for the various cases, *i.e.*

$$\check{Q}(U) = - \text{sign}(U) \cdot \quad (2.67)$$

$$\begin{cases} \sqrt{2\varepsilon_0(1+\chi)(\check{p}^{\text{mat}}(U) - p^{\text{bulk}})} & \text{for Case 0 ,} \\ \sqrt{2\varepsilon_0(1+\check{\chi}(U))(\check{p}^{\text{mat}}(U) - p^{\text{bulk}} - \rho\psi^{\text{pol}}(|\check{E}(U)|) - \frac{\varepsilon_0}{2}\check{\chi}(U)|\check{E}(U)|^2)} & \text{for Case 1 ,} \\ \sqrt{2\varepsilon_0 \frac{(1+\check{\chi}(U))^2}{1+2\check{\chi}(U)} (\check{p}^{\text{mat}}(U) - p^{\text{bulk}})} & \text{for Case 2 and 3 .} \end{cases}$$

3 Discussion of the model

The non-constant susceptibility χ has a profound impact on the structure of the mathematical model derived in Sect. 2 above. Most notably, the Poisson equation (2.52a) is no longer semi-linear, but in general becomes quasi-linear. Moreover, additional non-linear force terms appear in the momentum balance (2.40b) or (2.42b) if χ depends on the local species concentrations. In the 1D system (2.59) this results in a much stronger non-linear coupling of the equations. In the following, we discuss the relation and structural differences to existing models from the literature, as well as different formulations of the momentum balance and the contributing forces.

3.1 Comparison with some existing models

Gouy-Chapman (GC) model The most simple model for the double layer is the Gouy-Chapman (GC) model based on the assumption of constant susceptibility χ and a Boltzmann distribution of ions in strongly diluted solutions. Considering a completely dissociated 1 : 1 electrolyte of bulk concentration c , the diffuse layer in front of a planar electrode surface at $z = 0$ is determined by the single semi-linear second order equation

$$-(1 + \chi)\varepsilon_0 \partial_{xx}\varphi = \hat{q}(\varphi) = 2e_0c \sinh\left(\frac{e_0}{k_B T}\varphi\right), \quad (3.1)$$

such that $\varphi \rightarrow 0$ and $\partial_x\varphi \rightarrow 0$ for $z \rightarrow \infty$. The equivalent first order system for the 1D setting is

$$E = -\partial_x\varphi, \quad (3.2a)$$

$$\partial_x(\varepsilon_0(1 + \chi) \cdot E) = \hat{q}(\varphi). \quad (3.2b)$$

The boundary layer charge and the differential capacitance according to the GC model are given by

$$Q_{GC}(E) = -2\sqrt{2c \cdot (1 + \chi)\varepsilon_0 k_B T} \cdot \sinh\left(\frac{e_0}{2k_B T}(E - E^{\text{PZC}})\right), \quad (3.3a)$$

$$C_{GC}(E) = -\sqrt{2c \cdot \frac{(1 + \chi)\varepsilon_0 e_0^2}{k_B T}} \cdot \cosh\left(\frac{e_0}{2k_B T}(E - E^{\text{PZC}})\right), \quad (3.3b)$$

where E^{PZC} denotes the potential of zero charge (PZC). Comparing with experimental data of [49], the GC model strongly overestimates the boundary layer charge already for small applied voltages ¹ and

¹As a consequence of the strong dilution assumption, there is no mechanism in the GC model to define an upper limit for the accumulation of charge. This is also compatible with the conception of ions as point charges.

predicts an U-shape of the capacitance, in disagreement with the curves in Fig. 2. However, very close to the PZC, the GC model can be expected to be reasonably well applicable. In order to roughly fit the GC model to the local capacitance minima at a Ag (110) surface according to [49], see Fig. 2, there is only one parameter, i.e. the (constant) susceptibility χ . Such a fit would result in $\chi \approx 40$, very different from what should be expected in the electrolyte bulk, i.e. $\chi \approx \chi_S \approx 80$, and similar order as in rather concentrated solutions according to [30, 11], cf. Fig. 1.

Gouy-Chapman-Stern-Grahame (GCSG) model. If one wants to keep the simple description of a diffuse layer by the GC model, one can try to circumvent the problem of unreasonable charge accumulation by inverting the charge vs. applied potential relation. As a result, the GC theory then only opens a very narrow window for the potential drop across the diffuse layer. In order to close the remaining gap to the actual applied potential, an inner part of the double layer (Helmholtz layer) is introduced, which is thought to behave like a plate capacitor. Then, the resulting GCSG model expresses the total capacitance of the double layer as

$$(C_{\text{GCSG}}(Q, c))^{-1} = (C_i(Q))^{-1} + (C_d(Q, c))^{-1}, \quad (3.4)$$

It is commonly postulated that inner layer capacitance C_i is independent of the bulk concentration and diffuse layer capacitance is given by GC capacitance with the susceptibility of pure water, i.e. $C_d = C_{GC}$ with $\chi = 80$. The GCSG model allows good qualitative and quantitative agreement with experimental data [49], see also [29]. However, the GCSG model needs as an empirical input parameter a complete inner layer capacitance curve C_i , which is an input of the same type as the desired output of the model.

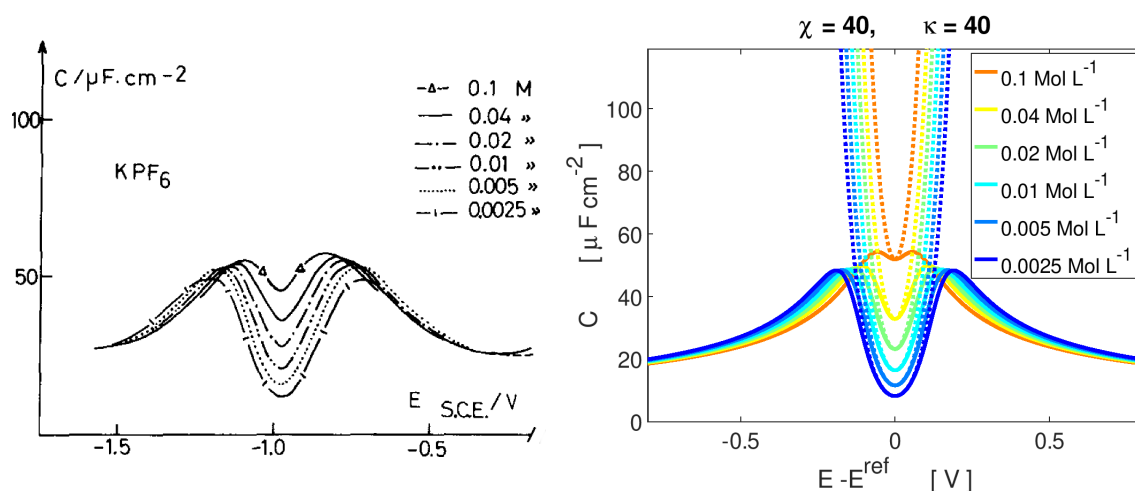


Figure 2: Left: Differential capacitance for a Ag(110) surface (Fig. 3 of [49]). Right: Computed capacitance with constant χ (solid lines) and Gouy-Chapman for comparison (dotted).

Steric Poisson-Nernst-Planck (sPNP) models. The most striking deficiency of the GC model is the missing limitation of the local ion concentration, due to the strong dilution assumption. To cure this problem, lattice gas models introducing a size parameter have been proposed in order to account for finite ion size in [32, 10, 3]. We further on refer to these models as Bikerman models. Extensions to multiple different ion sizes are e.g. [13, 35, 36]. Independently, a general continuum model –here called DGML model– that is based on non-equilibrium thermodynamics and takes finite ion size and ion solvation into account was introduced in [19, 34, 20]. While the mathematical structure of the

Bikerman model is still the same as (3.1), only with a different function $\hat{q}(\varphi)$, the DGLM model in the incompressible case corresponds to the Case (0) above and the system (2.52) takes the form

$$-(1 + \chi)\varepsilon_0\Delta\varphi = \hat{q}(\varphi, p) = e_0 \frac{\sum_{\alpha \in \mathcal{I}} z_\alpha y_\alpha(\varphi, p)}{\sum_{\alpha \in \mathcal{I}} v_\alpha^E y_\alpha(\varphi, p)} \quad \text{with} \quad (3.5a)$$

$$1 = \sum_{\alpha \in \mathcal{I}} y_\alpha(\varphi, p) = \sum_{\alpha \in \mathcal{I}} y_\alpha^{\text{bulk}} \exp\left(-\frac{z_\alpha e_0}{k_B T}(\varphi - \varphi^{\text{bulk}}) - \frac{v_\alpha^E}{k_B T}(p - p^{\text{bulk}})\right), \quad (3.5b)$$

In the case that the specific volume v_α^E is the same for all species, in particular if solvation of ions is not considered, the pressure can be eliminated from the Poisson equation and the DGLM model reduces to the the Bikerman case.

The steric Poisson-Nernst-Planck models are capable to reproduce experimental data in a qualitative manner, including a transition from the camel shape for dilute solutions to a bell shape curve for large bulk salt concentrations. To reach also agreement with the experiments in the correct quantitative range for a wide range of bulk salt concentrations and applied potentials, the parameters of the DGLM model were fitted in [34] as $\chi = 25$ and v_α^E of the ionic species such that it contains 45 times the specific volume of the solvent. The constant susceptibility should be interpreted as an effective value relevant for concentrated solutions, although we note that this value is lower than experimentally observed in [30, 11].

Models with non-constant χ . To account for the electric field dependence of χ , i.e. the dielectric saturation, Bikerman type models have been introduced. In [4], $\chi(|E|)$ according to Graham [27] is considered and in particular for $m = 1/2$, that corresponds to our (2.43a), analytical solutions are derived. Following [15, 43, 9] with the Langevin function as in (2.43b). a Poisson-Boltzmann approach was proposed in [26], Bikerman models are provided in [25, 7], an extension to different ion sizes is derived [24]. The mathematical structure of the Bikerman models with $\chi(|E|)$ is only changed by the higher order nonlinearity on the left hand side of the poisson equation.

Bikerman type which account for the concentration dependence with linear dielectric decrement are developed in [6, 31, 42, 21] and extended to different ion sizes in [28]. In the function \hat{q} on the left hand side of the Poisson equation, there are terms introduced that are proportional to $|E|^2$, reflecting the electric field dependence of the chemical potentials for concentration dependence of χ , in particular in our Case 2 above.

3.2 Discussion of momentum balance

As already noted in Sect. 2.2, a discussion of forces in the momentum balance always requires the reference to the stress tensor that they are related to. Coupling of the electric field to the thermodynamics of matter leads to a Lorentz force $q^E \mathbf{E}$ with $q^E = \text{div}(\varepsilon_0 \mathbf{E})$ [48, 41, 20]. For a constant susceptibility χ , the Lorentz force can easily be written as $q \mathbf{E}$ by modifying the stress tensor by χ times the Maxwell stress tensor. In the momentum balance (2.4c), we chose to put a force term $(\nabla \mathbf{E}) \mathbf{P}$ on the right hand side. This force is referred to as *Kelvin polarization force*, cf. [39, Sect. 3.6 eqn. (5)], or *ponderomotive force*, cf. [16]. although often the term ponderomotive force is used to refer to a force on a dielectric in an oscillating electromagnetic field of high frequency. In the setting of Sect. 2.2, this explicit force term is favorable because then the representation of the stress tensor reduces from (2.9d) to $\boldsymbol{\sigma} = \left(\rho\psi - \sum_{\alpha \in \mathcal{I}} n_\alpha \mu_\alpha\right) \mathbf{1} + \boldsymbol{\sigma}^{\text{visc}} + \boldsymbol{\sigma}^{\text{pol}}$ whereby for homogeneous dependency of χ on n_α , i.e. in Cases 2 and and Case 3, the stress $\boldsymbol{\sigma}$ in equilibrium becomes

completely independent of the electromagnetic field. However, the Kelvin force $(\nabla \mathbf{E})\mathbf{P}$ does not necessarily vanish in Case 0 of constant χ , since the gradient acts on \mathbf{E} and not on \mathbf{P} . In fact, in Case 0 and Case 1, the Kelvin force term is canceled in equilibrium by the polarization pressure because then $\nabla p^{\text{pol}} = -\nabla \rho \psi^{\text{pol}} = (\nabla \mathbf{E}^{\text{Eq}})\mathbf{P} = (\nabla \mathbf{E})\mathbf{P}$.

The forces in (2.9d) can be rewritten as

$$q \mathbf{E} + (\nabla \mathbf{E})\mathbf{P} = q \mathbf{E} + \frac{1}{2} \nabla (\chi |\mathbf{E}|^2) - \frac{1}{2} |\mathbf{E}|^2 \nabla \chi, \quad (3.6)$$

where last term represents a force that is present whenever χ is not constant. Moreover, in Case 2 we have by definition $p^{\text{pol}} = \frac{1}{2} \hat{\chi}^{(2)} |\mathbf{E}|^2 - \frac{1}{2} |\mathbf{E}|^2 \sum_{\alpha \in \mathcal{I}} n_{\alpha} \frac{\partial \hat{\chi}^{(2)}}{\partial n_{\alpha}}$ such that in the momentum balance (2.30) written in terms of ∇p^{mat} instead of ∇p we have the forces

$$q \mathbf{E} + (\nabla \mathbf{E})\mathbf{P} - \nabla p^{\text{pol}} = q \mathbf{E} + \frac{1}{2} \nabla \left(|\mathbf{E}|^2 \sum_{\alpha \in \mathcal{I}} n_{\alpha} \frac{\partial \hat{\chi}^{(2)}}{\partial n_{\alpha}} \right) - \frac{1}{2} |\mathbf{E}|^2 \nabla \hat{\chi}^{(2)}, \quad (3.7)$$

where the second term on the right hand side is called *electrostrictive* force. This form of the force terms can be found e.g. in [5, eqn. (3.4.9)], [22, eqn. (4.89)], or in [39, Sect. 3.7 eqn. (24)] where the last two terms together are referred to as electric Korteweg-Helmholtz force density. Contrary to the present paper, the electrostrictive force of (3.7) is neglected in [39, Sect. 3.7 eqn. (22)] for incompressible media. For the analysis of electric-mechanic coupling in double layer capacitors, a Cauchy-Poisson system is considered in [40, eqn. (8)] where the electrostrictive force is neglected. However, the momentum balance is mostly used to derive boundary conditions at the electrode electrolyte interface.

4 Material properties of the electrolyte

In this section we investigate an incompressible electrolytic solution with water as solvent and some monovalent salt AC, which is subject to the dissociation reaction (2.2) with $\nu_A = \nu_C = 1$. We consider a mixture of the 4 species solvent S, solvated anions A, solvated cations C and ion pairs AC.

We seek to investigate an electrolytic solution where the electrolyte concentration c [mol L⁻¹] is a parameter that is varied in our study. The electrolyte can be characterized by the bulk concentration c and the dissociation degree δ defined by

$$c = \left(n_{AC}^{\text{bulk}} + \frac{1}{2} (n_A^{\text{bulk}} + n_C^{\text{bulk}}) \right) \cdot \frac{1}{1000 \mathcal{N}_A}, \quad n_{AC}^{\text{bulk}} = (1 - \delta) c \cdot 1000 \mathcal{N}_A. \quad (4.1)$$

Electro-neutrality of the bulk,

$$n_A^{\text{bulk}} = n_C^{\text{bulk}} = \delta \cdot c \cdot 1000 \mathcal{N}_A. \quad (4.2)$$

The dissociation degree $\delta = \hat{\delta}(c)$ is determined from the equilibrium condition (2.13a) for the reaction (2.2). Given the material model of Sect. 2.3, it depends on the solvation numbers κ_A, κ_C and the Gibbs energy $\Delta g := \psi_A^{\text{E}} + \psi_C^{\text{E}} - \psi_{AC}^{\text{E}} - (\kappa_A + \kappa_C) \psi_S^{\text{E}}$ of the dissociation reaction.

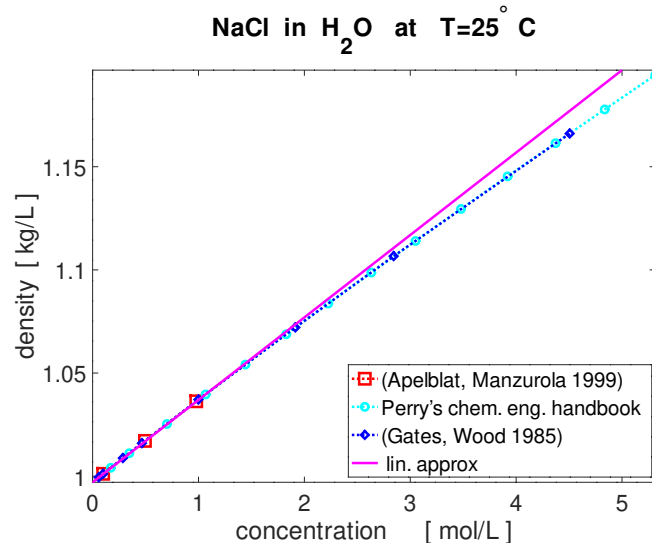


Figure 3: Experimental data for the density of NaCl as function of the salt concentration.

4.1 Bulk mass density and specific volumes.

Experimental observations, e.g. [23, 2, 44], show that the mass density $\rho = \sum_{\alpha} m_{\alpha} n_{\alpha}$ of the electrolyte is approximately a linear function of the salt concentration c , see Fig. 3.² We obtain

$$\rho = \rho_S^0 + \left(m_{AC} + (\kappa_A + \kappa_C - \frac{(v_A + v_C)}{v_S}) m_S \right) n_A + \left(m_{AC} - \frac{v_{AC}}{v_S} m_S \right) n_{AC} \quad (4.3)$$

where ρ_S^0 denotes the mass density of the pure solvent. The molar mass of a solvated ion is $m_{\alpha} = m_{\alpha}^0 + \kappa_{\alpha} m_S$, where m_{α}^0 denotes the molar mass of the bare central ion. While mass is conserved upon dissolution and dissociation of the salt in the liquid solvent, the partial molar volume is not necessarily. Hence we consider the decomposition

$$v_{\alpha}^E = v_{\alpha}^0 + \kappa_{\alpha} v_S^0 + v_{\alpha}^{Ex}, \quad \alpha = A, C, \quad (4.4)$$

and for the ion pair, similarly, $v_{AC}^E = v_{AC}^0 + v_{AC}^{Ex}$, where $v_{AC}^0 = v_A^0 + v_C^0$ and $v_{AC}^0 = \frac{m_{AC}}{\rho_{AC}^0}$ with ρ_{AC}^0 as density of the solid salt. This yields

$$\rho = \rho_S^0 + m_{AC} \left(1 - \frac{\rho_S^0}{\rho_{AC}^0} \right) \cdot c - \rho_S^0 (v_A^{Ex} + v_C^{Ex}) \delta \cdot c - \rho_S^0 v_{AC}^{Ex} (1 - \delta) \cdot c, \quad (4.5)$$

where c is the salt concentration and δ the dissociation degree. If $v_A^{Ex} + v_C^{Ex} = v_{AC}^{Ex}$, the dissociation degree drops out of the expression for the mass density ρ and the volume is conserved during the dissociation reaction (however, not during the dissolution reaction), i.e. $(v_A^E + v_C^E) = v_{AC}^E + (\kappa_A + \kappa_C) v_S^E$, which we assume for the sake of this work. We can fit v_{AC}^{Ex} to experimental data, yielding for NaCl a value of $v_{AC}^{Ex} = -0.0081 [\text{Lmol}^{-1}]$, and emphasize that the solvation number κ yet remains an independent parameter.

²Here, concentration is consistently calculated from experimental data given in molality or weight percent.

4.2 Bulk concentration dependent susceptibility

The material model (2.40a) for the susceptibility yields together with the incompressibility constraint (2.29) the relation

$$\chi = \chi_S - \sum_{\alpha \in \mathcal{I} \setminus S} (\chi_S - \chi_\alpha) v_\alpha^E n_\alpha^{\text{bulk}}. \quad (4.6)$$

For a completely dissociated salt AC of concentration c , we obtain

$$\text{for } \delta = 1: \quad \chi = \chi_S - d \cdot c \quad \text{with} \quad d = (\chi_S - \chi_A) v_A^E + (\chi_S - \chi_C) v_C^E, \quad (4.7)$$

which reflects naturally the experimental observation of a linear decrease up to a certain concentration, *c.f.* Fig. 4.

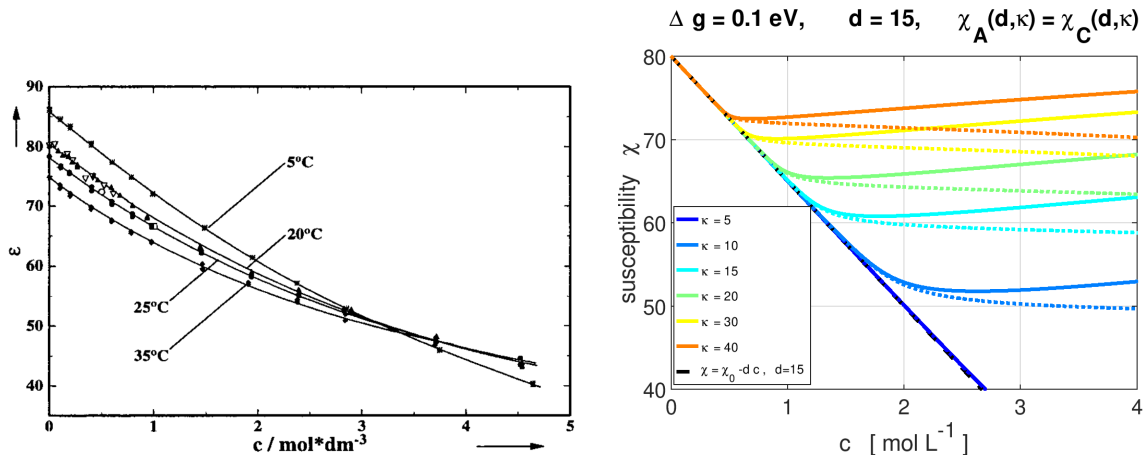


Figure 4: Left: concentration dependent susceptibility (dielectric decrement) (Fig. 2 of [11]). Right: Susceptibility according to the model (4.6) as function of the salt concentration c for different values of d .

With $\chi_A = \chi_C$ and the same assumptions as in the previous paragraph, i.e. $\kappa_A = \kappa_C = \kappa$ and $v_A^E = v_C^E = 0.5v_{AC}^E + \kappa v_S^E$, we obtain the constraint

$$\chi_A = \chi_S - \frac{d}{(v_{AC}^E + 2\kappa v_S^E) 1000 \mathcal{N}_A}, \quad (4.8)$$

which is a function of the solvation number κ and plotted in Fig. 5 for various values of d . We observe that already a small dielectric decrement of $d = 5$ requires a positive solvation number $\kappa \geq 2$. On the other hand, a solvation κ number larger than 20 requires a susceptibility coefficient $\chi_A \geq 50$ in order to maintain a decrement not exceeding $d = 20$.

If not stated otherwise, we use a value of $d = 15$ for the following numerical simulations.

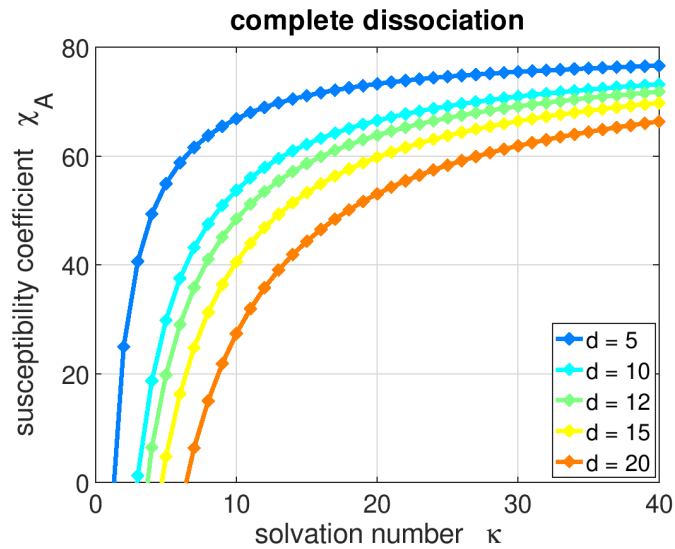


Figure 5: Coefficient $\chi_A = \chi_C$ according to (4.8) in dependence of κ for different values of the dielectric decrement d .

4.3 Incomplete dissociation

Beyond a certain concentration value, which is dependent on the solvation number κ [33], incomplete dissociation becomes crucial, which implies ion pairs AC as additional species in the electrolyte. For an incompletely dissociated salt AC of concentration c , we obtain for the bulk susceptibility

$$\text{for } \delta = \hat{\delta}(c): \quad \chi = \chi_S - d_1 \cdot c \cdot \hat{\delta}(c) - d_2 \cdot c \cdot (1 - \hat{\delta}(c)) \quad (4.9)$$

$$\text{with } d_1 = (\chi_S - \chi_A)v_A^E + (\chi_S - \chi_C)v_C^E, \quad d_2 = (\chi_S - \chi_{AC})v_{AC}^E \quad (4.10)$$

where $\delta = \hat{\delta}(c)$ is determined from the algebraic condition (2.56), which yields a non-linear relation for χ in terms of c . In Fig. 6 the dissociation degree $\delta(c)$ is plotted from the dissociation equilibrium (2.13a) for the reaction (2.2) based on the material model of a simple mixture of solvated ions for $\Delta g = 0.1$ eV and in dependence of the solvation number as a parameter. Larger solvation numbers κ result in a lower dissociation degree. Smaller values of Δg move the curves to the left such that incomplete dissociation is observed at lower concentrations, whereas larger values of Δg move the curves to the right. At a value of $\Delta g = 0.1$ eV, the electrolyte solution can be considered as completely dissociated for concentrations almost up to $c = 1 \text{ mol L}^{-1}$ if the solvation number $\kappa \leq 20$.

The concentration dependent susceptibility χ based on incomplete dissociation with $\Delta g = 0.1$ eV is plotted in Fig. 6 for different values of κ . For low concentrations, where $\delta \approx 1$, $\chi(c)$ follows the straight line with slope $-d$. Then, depending on κ , the slope of the curves decreases, leading to $\chi > \chi_S - dc$. Thus far, the coefficient χ_{AC} for the ion pair is not specified. Since a free ion pair could be associated with a large dipole moment, it might be reasonable to assume $\chi_{AC} \approx \chi_S$. This choice corresponds to the solid lines in Fig. 6. A lower bound of χ is given by the choice $\chi_{AC} = 0$, related to the dotted lines. We observe that for $\kappa \geq 20$, the concentration dependent χ is always larger than 60.

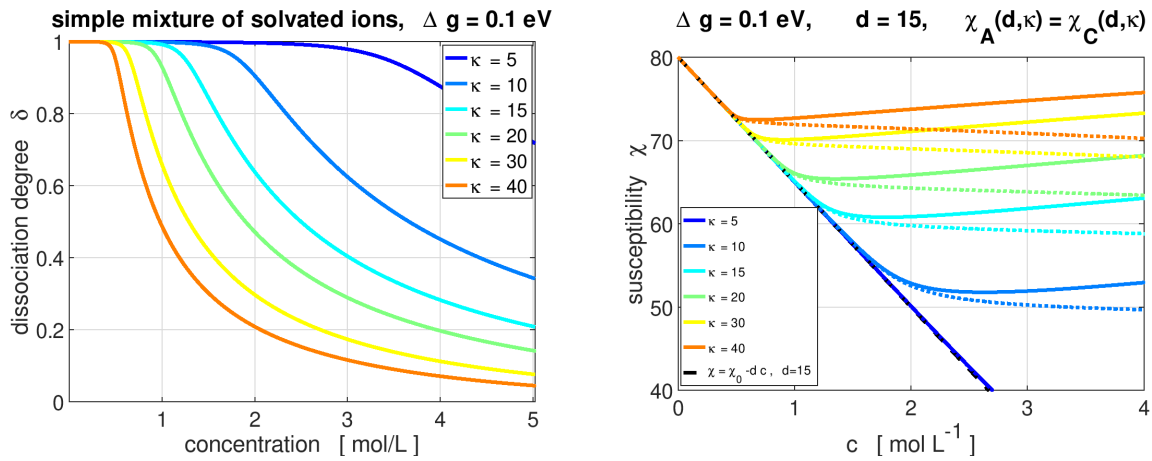


Figure 6: Left: dissociation degree over concentration for different κ . Right: concentration dependent susceptibility over concentration for different κ , solid lines with $\chi_{AC} = \chi_S = 80$, dotted lines with $\chi_{AC} = 0$.

4.4 Field dependent susceptibility in boundary layers

The examples in Sect. 2.3 for non-linear functions of the susceptibility with respect to the electric field strength contains a dimension afflicted parameter a , i.e. for (2.43a) we have

$$\chi = \frac{\chi_S}{\sqrt{1 + \tilde{a}|\mathbf{E}|^2}}. \quad (4.11)$$

Within a natural non-dimensionalization of the electrostatic potential and the space dimension, a reference field strength $E^0 = \frac{k_B T}{e_0} \cdot (1 \text{ nm})^{-1} \approx 2.6037 \times 10^7 \text{ Vm}^{-1}$ arises whereby it is convenient to introduce the the unscaled parameter $a := \frac{\tilde{a}}{(E^0)^2}$. Then a choice of the parameter a is then in comparable order to values found in the literature, cf. Fig. 7. E.g. [27] proposes (2.44) with $\tilde{a}/2 = 1.2 \times 10^{-17}$, while [37, (eqn. 25)] suggests (2.44) for $m = 1$ with a slightly different constant $\tilde{a}/2 = 1.443 \times 10^{-17}$, but also refers to computed values of [14], although they are not in good agreement with this choice of parameter. If not stated otherwise, we use a value of $a = 0.01$ for the following numerical simulations.

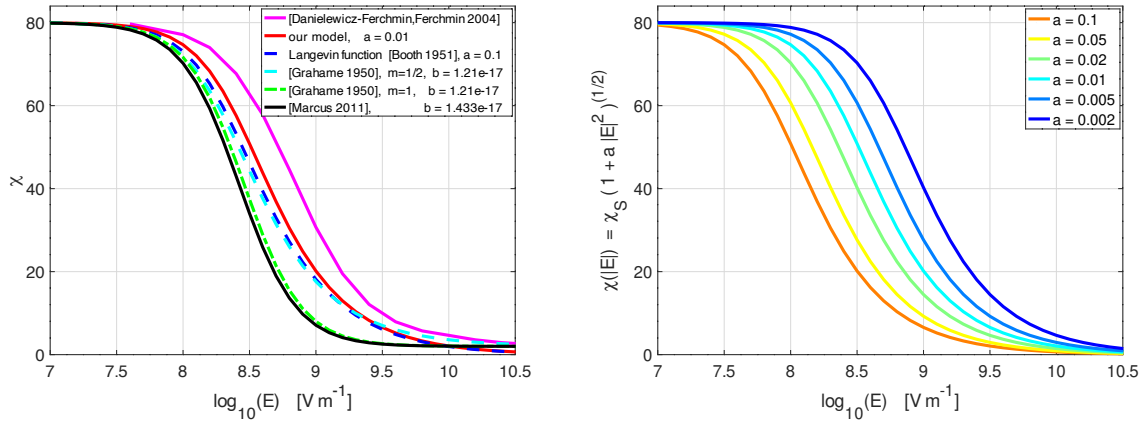


Figure 7: Left: Comparison of different models for dielectric saturation. Right: $\chi(|\mathbf{E}|)$ according to (2.43a) for different values of the parameter \tilde{a} .

4.5 Concentration and field dependent susceptibility

For the general case of a concentration and field dependent susceptibility, *i.e.*

$$\chi = \sum_{\alpha \in \mathcal{I}} v_{\alpha}^{\text{E}} n_{\alpha} \cdot \chi_{\alpha}(|\mathbf{E}|^2) \quad (4.12)$$

we consider exemplarily an extension of 4.4 for each species, that is

$$\chi_{\alpha} = \frac{\chi_{\alpha}^0}{\sqrt{1 + \tilde{a}_{\alpha} |\mathbf{E}|^2}}. \quad (4.13)$$

Similar to 4.4, the natural non-dimensionalization of the electric field yields the dimensionless parameter $a_{\alpha} := \frac{\tilde{a}_{\alpha}}{(E^0)^2}$. We choose the parameter a_S similar to 4.4, *i.e.* $a_S = 0.01$, and discuss ratios of $a_A = A_C$ to a_S (see Fig. 8).

The parameters χ_{α}^0 can be determined from the experimentally estimated dielectric decrement $d = 15$, and the partial molar volumes of the ionic species, *i.e.* from eq. (4.7), as

$$\chi_{\alpha}^0 = \chi_S^0 - \frac{d}{2 \cdot v_{\alpha}^{\text{E}}}, \quad \alpha = A, C \quad (4.14)$$

and χ_S^0 is the susceptibility of the pure solvent.

Much smaller values of $a_A = a_C$ compared to a_S yield a non-monotonic behavior of χ in terms of the electric field, while larger values of $a_A = a_C$ lead to a steeper decrease of the susceptibility. We explore the impact of this on the space charge layer in section 2.4.

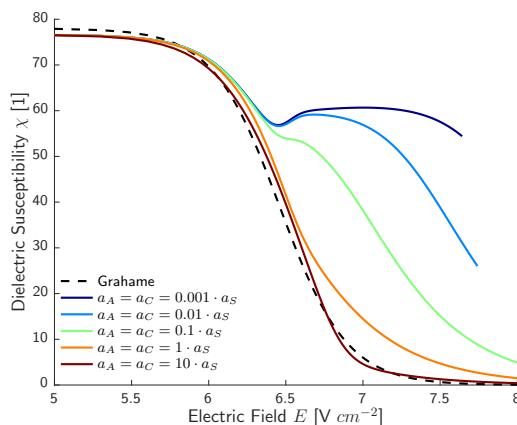


Figure 8: Field dependent susceptibility for various values of $a_A = a_C$ with $a_S = 0.01$.

5 Numerical study of the double layer and its differential capacitance

The spatial profile of the boundary layer is determined from the general system (2.52), or equally well from the ODE system (2.58) or (2.59) due to the 1D setting. For given applied potential, bulk electrolyte concentration and given parameters κ , d , a the spatial profiles of n_α , φ , p , χ are numerically computed. In the following boundary layer profiles are shown for an applied voltage of $E - E^E = 1$ V and bulk salt concentration of 0.01 mol L^{-1} . Then, from the given spatial profiles of the species number densities, the free charge is computed by numerical integration in order to determine the differential capacitance of the double layer. The obtained results have been confirmed by subsequent evaluation of the algebraic relations (2.63) that do not require spatial resolution of the boundary layer.

Experimental measurements of the differential capacitance, like e.g. [49], are made in a range of electrolyte bulk concentration up to 0.1 mol L^{-1} neglecting the effect of incomplete dissociation or ion pair formation. Accordingly, we first study separately the effects of concentration and electric field dependence of the susceptibility χ under the assumption of complete dissociation. Then we combine both effects, still under the assumption of complete dissociation.

Electrolyte boundary layers are in general not dilute, but strongly concentrated or even saturated. Thus, we study in a further step the impact of incomplete dissociation. Spatially resolved boundary layers have been computed by a straightforward P1 finite-element-method for (2.52) using mass lumping. At the interface, a locally refined grid is used and Newton's method method is applied to solve the nonlinear system. The capacitance curves were computed from (2.67) by direct solution of nonlinear algebraic equation (2.62) with Newton's method and subsequent numerical differentiation with respect to the applied potential.

In addition, a reformulation of the Poisson-momentum equation system (2.42b) and (2.42c) together with the representation (2.47) of the mole fractions yields a system of non-linear ODEs $\vec{z}' = \vec{f}(\vec{z})$, i.e. a two-point boundary value problem (see Appendix A.3 for the derivation and the explicit representation). All simulation experiments were additionally carried out by a numerical solution of the equation system $\vec{z}' = \vec{f}(\vec{z})$ with Matlab[®] bvp4c solver, yielding the same results as our *in-house* P1 finite-element-method implementation. Hence all simulations were double checked with different numerical strategies, in addition to grid convergence, in order to present reliable numerical studies.

5.1 Impact of concentration dependence

To study the impact of the concentration dependent susceptibility, we vary the dielectric decrement d that characterizes the linear regime of low bulk electrolyte concentrations. Here, $d = 0$ corresponds to the case of constant susceptibility. Then, the coefficients $\chi_A = \chi_C$ are determined in dependence of the parameter κ according to (4.8).

Boundary layers. The potential difference between the electrolyte bulk and the electrode surface at $x = 0$ causes a boundary layer in the species concentrations, which in turn imply a boundary layer in the susceptibility χ .

In Fig. 9, we see that $\chi(x)$ gets locally reduced in the layer and approaches some rather flat plateaus in front of the electrode at $x = 0$. The observed plateau height decreases for increasing values d . Comparing the profiles of $\chi(x)$ for different values of the solvation number κ , we observe that the layer is, as could be expected from the constant case, less wide for $\kappa = 10$ than for $\kappa = 20$. Moreover, for the same value of d , χ attains lower level in front of the electrode for $\kappa = 10$. The minimal value of χ does not fall to values less than 40 when increasing d .

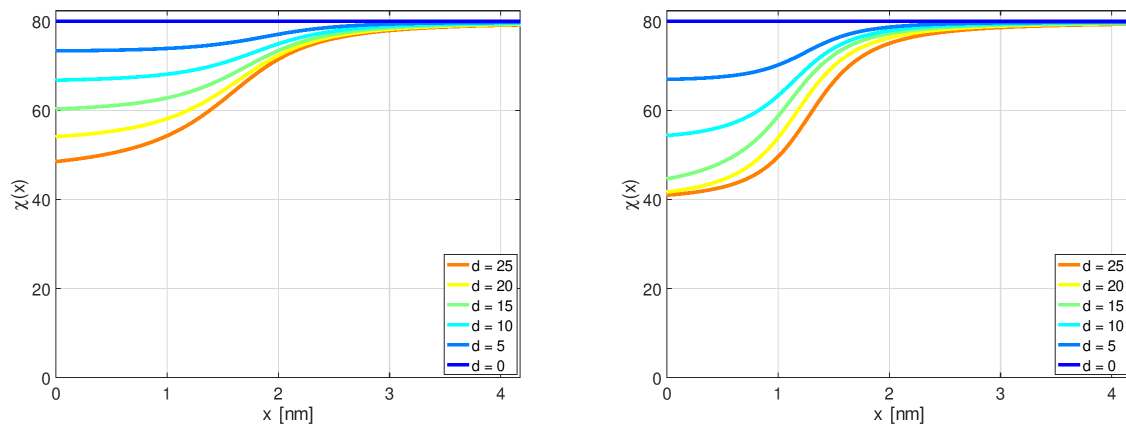


Figure 9: Profiles of the susceptibility χ in the boundary layer in dependence of d for $\kappa = 20$ (left) and for $\kappa = 10$ (right).

The profiles of the electric potential are not strongly influenced by the parameter d , see Fig. 10. For $\kappa = 20$, we observe a slightly faster decay of φ into the bulk when increasing d . However, in the case of $\kappa = 10$, this trend is only observed for $d \leq 15$, while for larger d the trend is reversed.

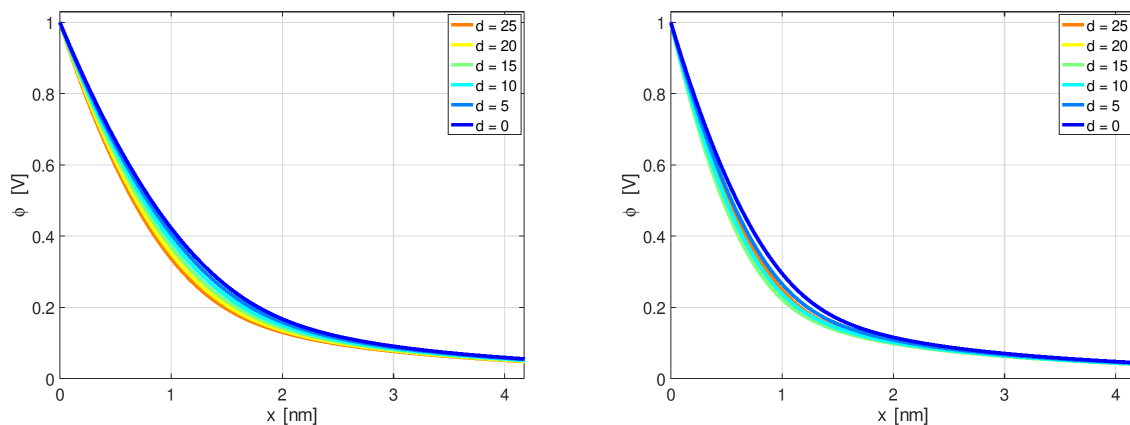


Figure 10: Profiles of the electric potential φ in the boundary layer do not strongly depend on d . Electric potential plotted for $\kappa = 20$ (left) and for $\kappa = 10$ (right).

Keeping the dielectric decrement fixed at $d = 15$ and increasing κ , confirms the previous observations that the layer width increases with κ and that the impact of the solvation parameter κ on the profile of the electric potential φ is more pronounced than the concentration dependence of χ , cf. Fig. 11. Moreover, Fig. 11 shows that the minimal value of χ decreases for decreasing κ and for $\kappa \geq 15$, these minimal values correspond to χ_A determined from (4.8) with $d = 15$, cf. Fig. 5.

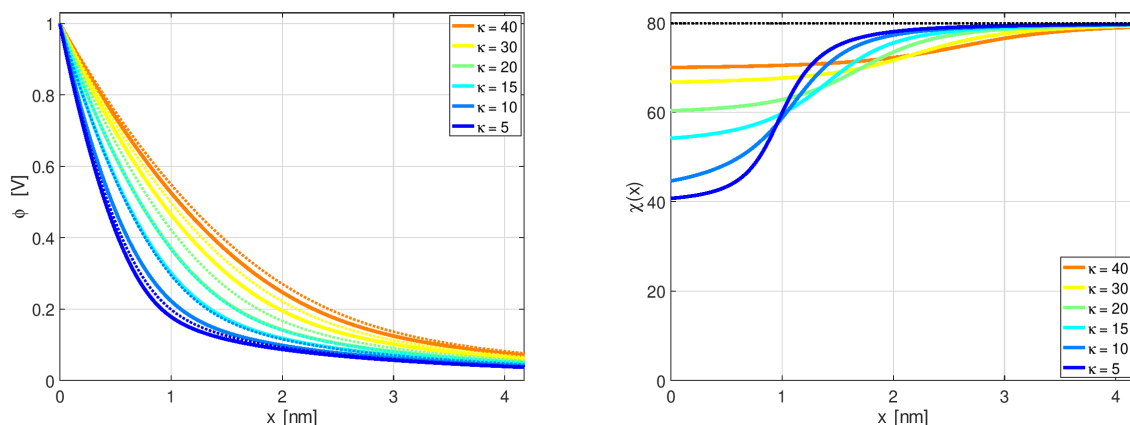


Figure 11: Boundary layer profiles of φ and χ for $d = 15$ and various values of κ . Dotted lines show the corresponding curves for constant $\chi = 80$. Left: layers of the electric potential get more wide for increasing κ . Right: Lower plateau height of χ in front of the electrode for smaller κ .

The difference in the qualitative behavior between $\kappa \leq 10$ and $\kappa > 10$ becomes most clear when looking at the boundary layer profiles of the number densities n_α . On the left hand side of Fig. 12, we observe that for $\kappa = 20$ the layers become slightly narrower when increasing d but the limiting values at the electrode surface at $x = 0$ are independent of d . While the solvent gets completely removed near the surface, the limiting concentration of the anions is determined by its specific volume v_A^E depending on κ as described in Sect. 4.1. To the contrary, we see on the right hand side of Fig. 12 that for $\kappa = 10$ and $d \geq 15$ the saturation level of n_α at $x = 0$ is lower than the value corresponding to ca. 5.5 mol L^{-1}

that could be expected from the specific volume v_A^E in these cases. Accordingly, the solvent gets not completely removed from the surface for $\kappa = 10$ and $d \geq 15$.

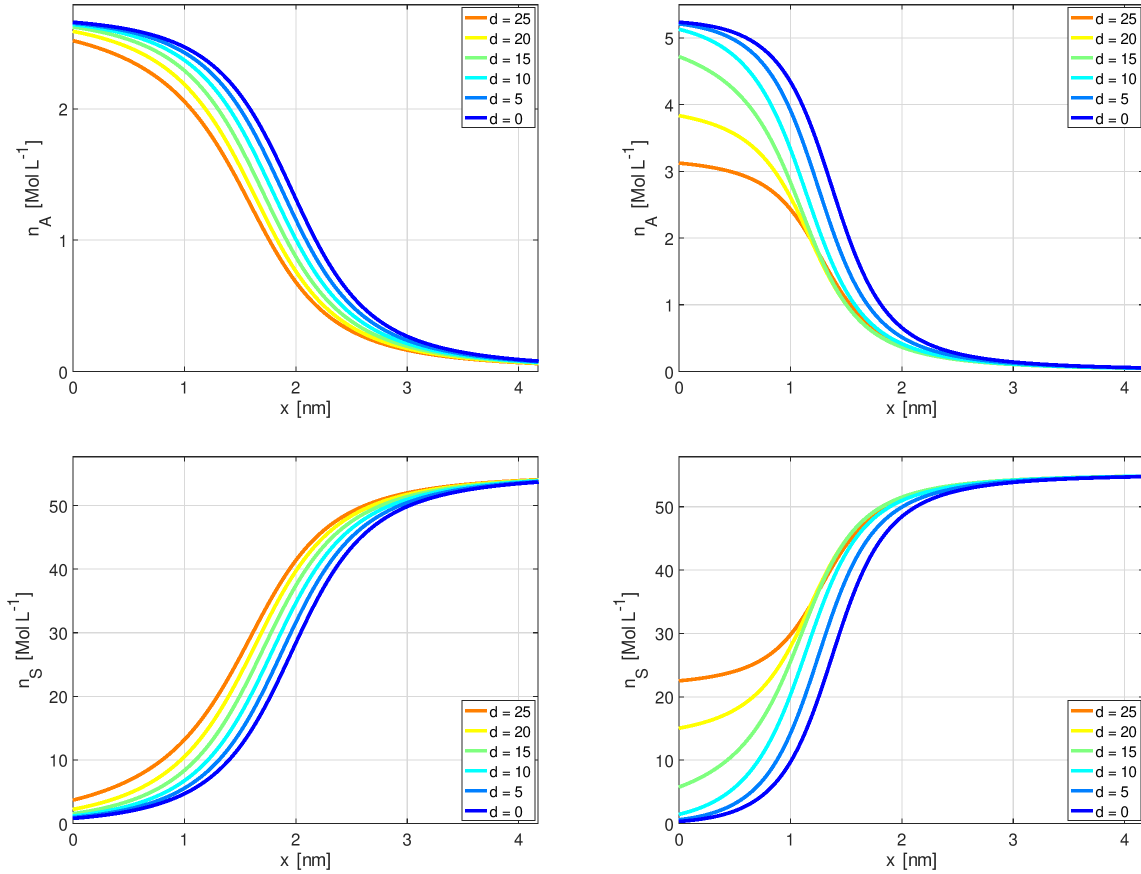


Figure 12: Boundary layer profiles of the number densities of anions n_A (top row) and solvent n_S (bottom row) for $\kappa = 20$ (left) and for $\kappa = 10$ (right) in dependence of the dielectric decrement d . The bulk electrolyte concentration is 0.01 mol L^{-1} and the applied voltage of $E - E^E = 1 \text{ V}$.

From the representation of the mole fractions y_α in the 1D case, one can deduce an estimate for the minimal level of the solvent concentration at the surface, i.e.

$$v_S^E n_S(x=0) \rightarrow \frac{1}{2} \max\left(0, \frac{\chi_S - 2\chi_A - 1}{\chi_S - \chi_A}\right) \quad \text{for } E - E^E \rightarrow \infty. \quad (5.1)$$

This relation is verified (numerically) in Fig.15. We observe that the solvent is completely removed from the surface if $d = 15$ and $\kappa = 10$ or larger.

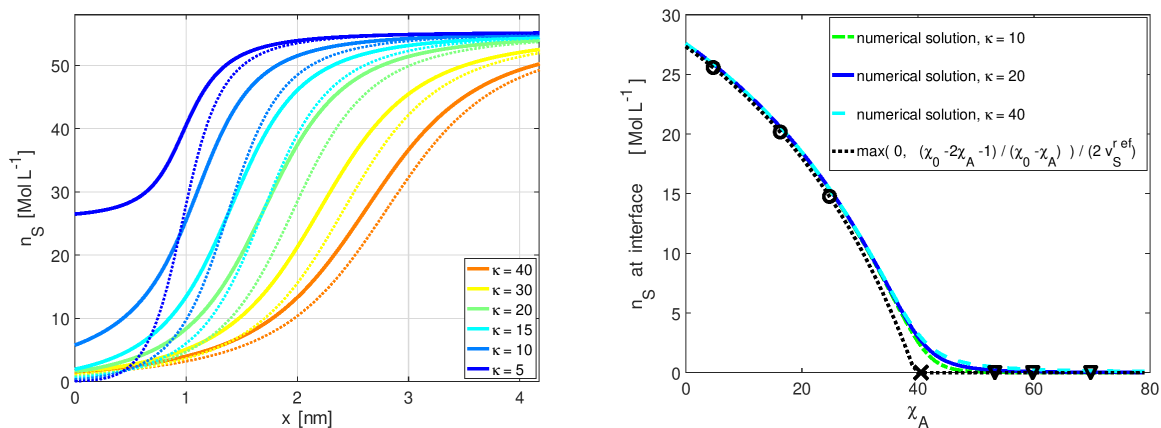


Figure 13: Left: boundary layer profiles of n_S for $d = 15$ and various κ (solid lines) and for comparison the corresponding curves for constant $\chi = 80$ (dotted lines). Right: limiting values of the solvent number density n_S at the surface $x = 0$ for large applied potentials as function of the coefficient χ_A . Values for χ_A according to (4.8) with $d = 15$ are given (from left to right) for $\kappa = 5, 6, 7$ (\circ), $\kappa = 10$ (\times) and $\kappa = 15, 20, 40$ (∇).

Differential capacitance. In Fig. 14 we observe that the concentration dependent susceptibility has an impact on the height of the capacity maxima of the interface. When d gets larger, the height of the maxima decreases for fixed bulk concentration and solvation number. At $d = 15$ and $\kappa = 10$, the maximal capacitance is about $100 \mu\text{Fcm}^{-2}$, what is considerably larger than typical observations in experiments.

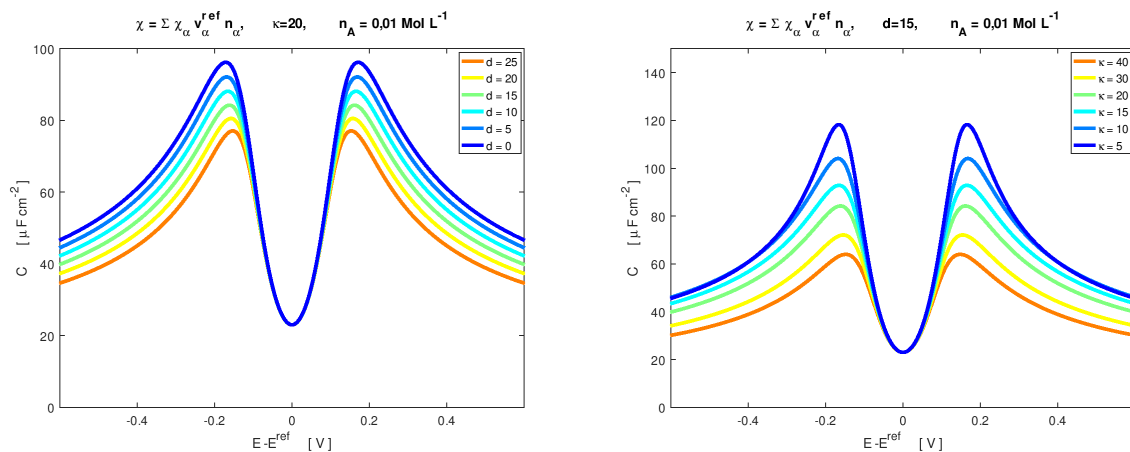


Figure 14: Differential capacitance for a bulk electrolyte concentration of 0.01 mol L^{-1} . Left: impact of varying dielectric decrement d , where $d = 0$ corresponds to the constant χ . Right: concentration dependent $\chi(c)$ with $d = 15$ for various values of κ .

Varying the solvation number κ , we observe the expected decrease of the capacitance maxima when increasing κ , as it is already known from the case of constant χ .

While both effects can be combined, increasing d and κ , it should be noted that for $\kappa = 30$ or larger, the effect of the concentration dependent χ , is not very pronounced any more. Neither of the parameters d

and κ has considerable impact on the height of the capacitance minimum at the PZC, as is analyzed in more detail in the next paragraph.

Equivalent susceptibility. For further comparison between concentration dependent $\chi(c)$ and the constant χ , we consider the parameter $\kappa = 10$ because the impact of the concentration dependence gets less pronounced larger values of κ .

We can determine a constant χ^{eff} such that for given applied potential and bulk concentration both models yield the same value for boundary layer charge Q . This is achieved with the algebraic relations in eq. (2.67), i.e. $\check{Q}^{(2)}(U; \chi^{\text{eff}}) \stackrel{!}{=} \check{Q}^{(0)}$, which is determined numerically. In Fig. 15 (left) we see that for applied potentials larger than 0.4 V the constant χ^{eff} depending on κ but not on the bulk concentration can be used. For $d = 15$ and $\kappa = 10$, then a simple model with constant $\chi^{\text{eff}} \approx 42$ can be used to obtain a boundary layer of approximately the same stored charge and similar width compared to the concentration dependent case. Fig. 15 shows that the approximating constant χ^{eff} is lower than the corresponding concentration dependent $\chi(d)$. Moreover, there is a notable difference in the material part of p^{mat} the pressure, which is much larger in the concentration dependent case. This difference is explained by the coincidence of the total pressure p in both cases and the vanishing $p^{\text{pol}} = 0$ for the material model of the homogeneously concentration dependent susceptibility. We note that such a difference in p^{mat} in the layer might become relevant when electro-osmotic flow is studied.

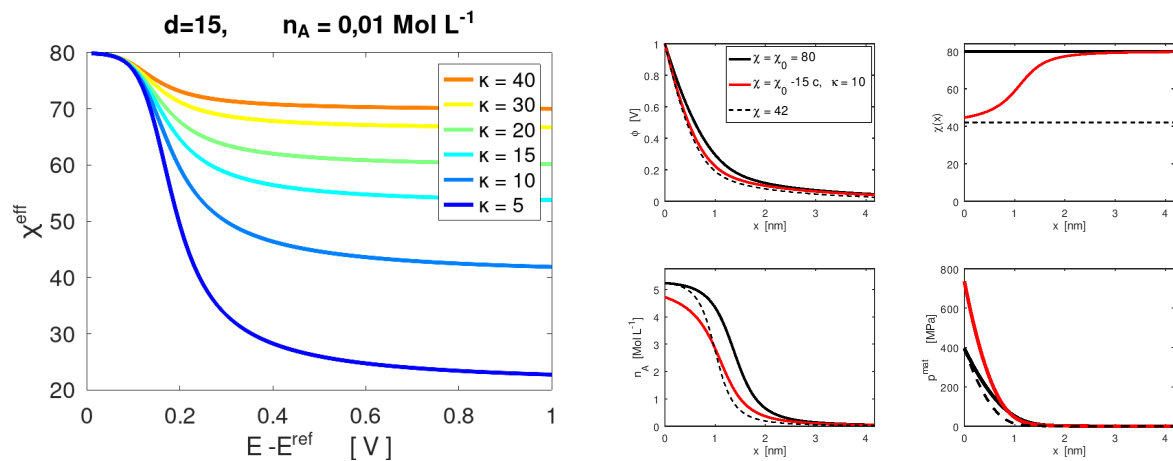


Figure 15: Left: effective constant susceptibility χ^{eff} over the applied potential $E - E^{\text{E}}$ to obtain the same boundary layer charge as in the case of $d = 15$ at a bulk concentration of 0.01 mol L^{-1} . Right: comparison of the boundary layer profiles for concentration dependent $\chi(c)$ with $d = 15$ and $\kappa = 10$ (red) and the cases of constant $\chi = 80$ (black solid), and choice of an effective constant $\chi = 42$ (black dashed).

5.2 Impact of field dependence

We consider the field dependence of the susceptibility according to the material law (2.43a). The results related to (2.43b) do not differ significantly from those presented below.

Boundary layers. In Fig. 16 we observe that the electric field dependence of the susceptibility results in spatial profiles of $\chi(x)$ that are more steep than in the case of concentration dependent susceptibility

analyzed before in Sect. 5.1. Expectably, χ tends to zero at $x = 0$ when the impact of the field dependency becomes significant, which occurs for $a > 0.002$.

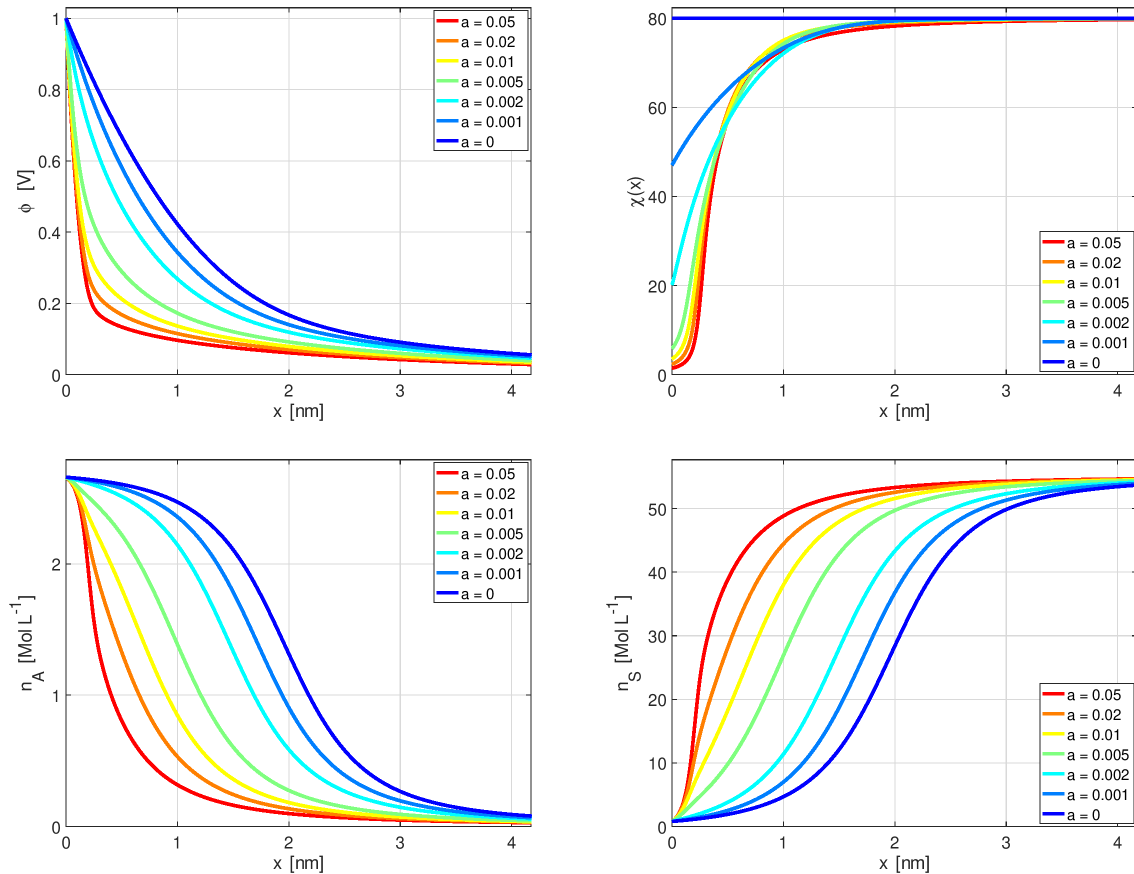


Figure 16: Profiles of in the boundary layer in dependence of a for $\kappa = 20$. The bulk electrolyte concentration is 0.01 mol L^{-1} and the applied voltage is $E - E^E = 1 \text{ V}$.

Because vanishing χ causes very steep decay of the electric potential φ , we observe that the impact of increasing the parameter a of the field dependency on the profiles of $\varphi(x)$ is very pronounced, see Fig. 16. Accordingly the layers in the species number densities n_α decrease in width when increasing the parameter a . The saturation levels of n_A and n_S are not affected by changes of a .

With respect to the solvation number κ , we observe again, as before in Sect. 5.1, that the layers are wider when parameter κ is larger.

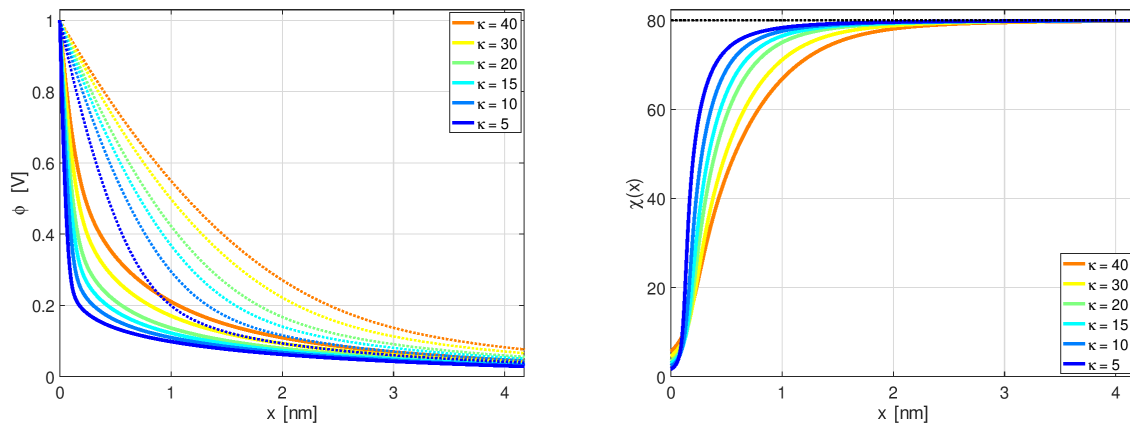


Figure 17: Profiles in the boundary layer for $a = 0.01$ (solid lines) and for constant $\chi = 80$ (dotted lines) for various values of κ . Left: layers of the electric potential get more wide and less steep for increasing κ . Right: χ always falls to nearly zero in front of the electrode with less steep layers for increasing κ .

Differential capacitance. The rapid decay of the susceptibility χ to almost 0 strongly reduces the capability of the boundary layer to store charge. Accordingly, once the local electric field is strong enough for the field dependence of χ to become relevant, the differential capacitance rapidly falls to nearly 0.

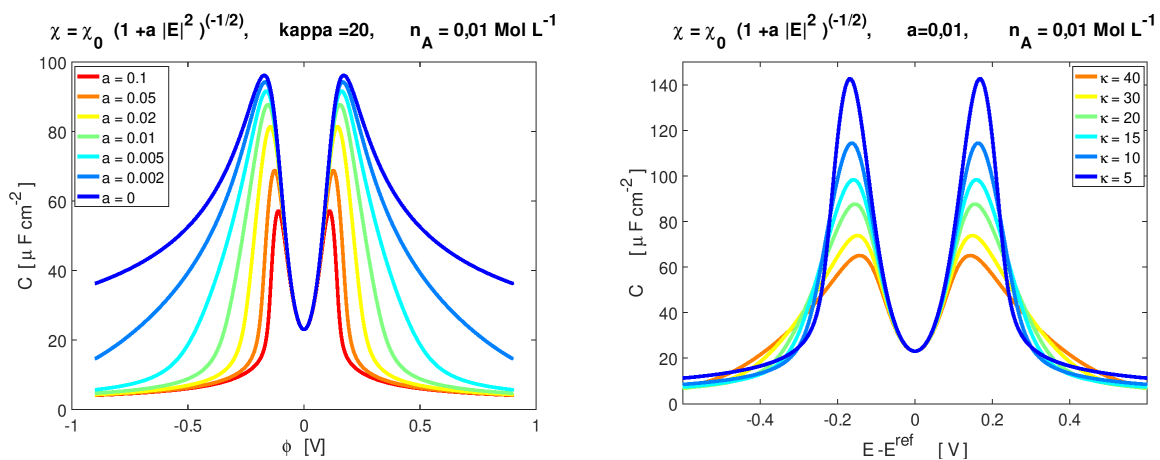


Figure 18: Differential capacitance for a bulk electrolyte concentration of 0.01 mol L^{-1} . Left: impact of varying the parameter a , where $a = 0$ corresponds to the constant χ . Right: field dependent $\chi(|E|)$ with $a = 0.01$ for various values of κ .

In Fig. 18 we observe that the field dependent susceptibility has an impact on the height of the capacity maxima of the interface. When a gets larger, the height of the maxima decreases for fixed bulk concentration and solvation number. At $a = 0.01$ and $\kappa = 20$, the maximal capacitance is about $90 \mu\text{F cm}^{-2}$, what is considerably larger than typical observations in experiments. Varying the solvation number κ , we observe the expected decrease of the capacitance maxima when increasing κ , as it is already known from the case of constant χ .

5.3 Concentration and field dependent susceptibility

For a fixed value $d = 15$ of the dielectric decrement, we study the impact of additional field dependence of the susceptibility.

Boundary layers. When combining the effects, the profiles of φ are, considerably steeper for increasing a , as observed before in Sect. 5.2, but are not strongly influenced by the value of d , as seen before in Sect. 5.1. χ

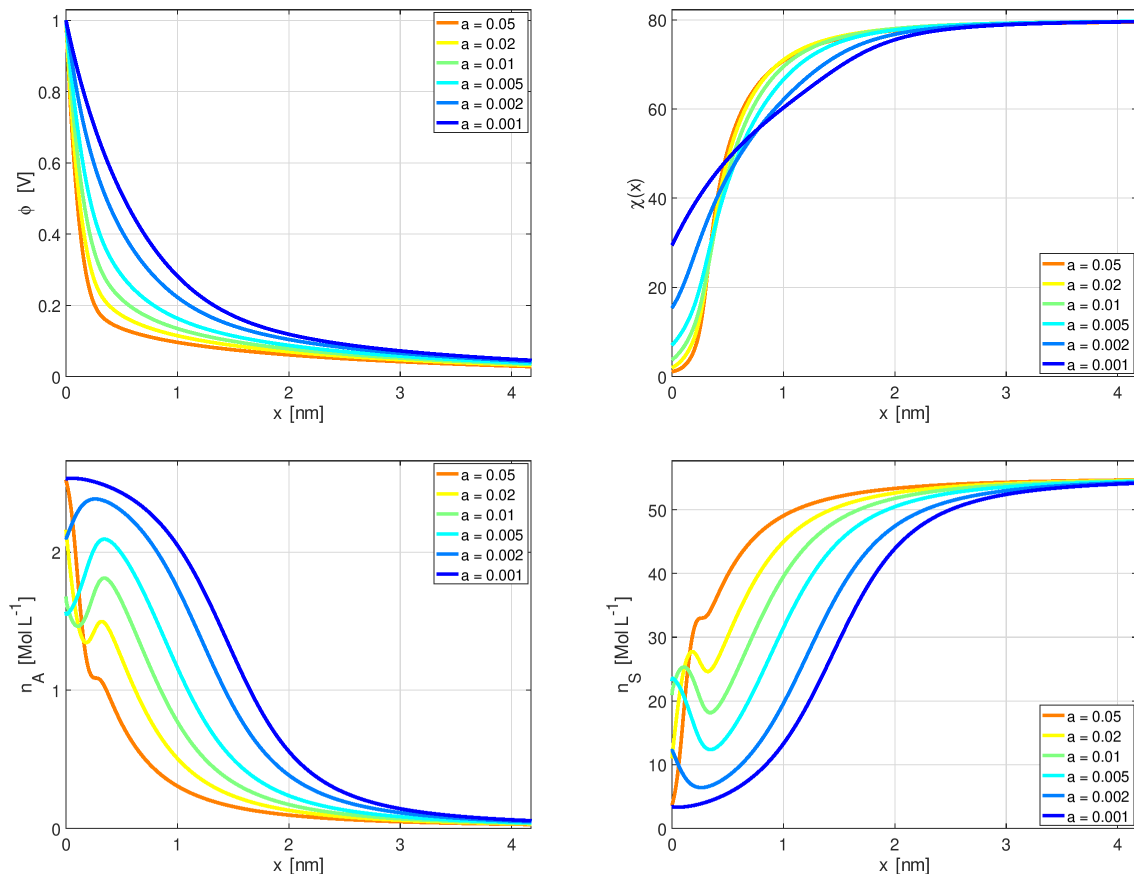


Figure 19: Profiles in the boundary layer for field and concentration dependent susceptibility χ for $\kappa = 20$ and various values of a at an applied voltage of $U = 1V$.

However, we observe a remarkable difference in the qualitative behavior of the profiles of the number densities, see Fig. 19, which shows computations for $a_S = a_C = a_S = a$ (c.f. section 4.4). While for a pure field dependency and for a pure concentration dependency of the susceptibility χ , as well as for $\chi = \text{const.}$, all species densities remain monotone in the electrochemical double layer, the combination of the both effects yields this new behavior of a non-monotone spatial species densities. The origin or interpretation of this effect is complex, but can be based on the momentum balance. As long as the electric field in the double layer is not too large, it is favorable for the solvent species to be pushed out of the double layer. This increases the local ionic concentration, which in turn, decreases locally the susceptibility (dielectric decrement - concentration).

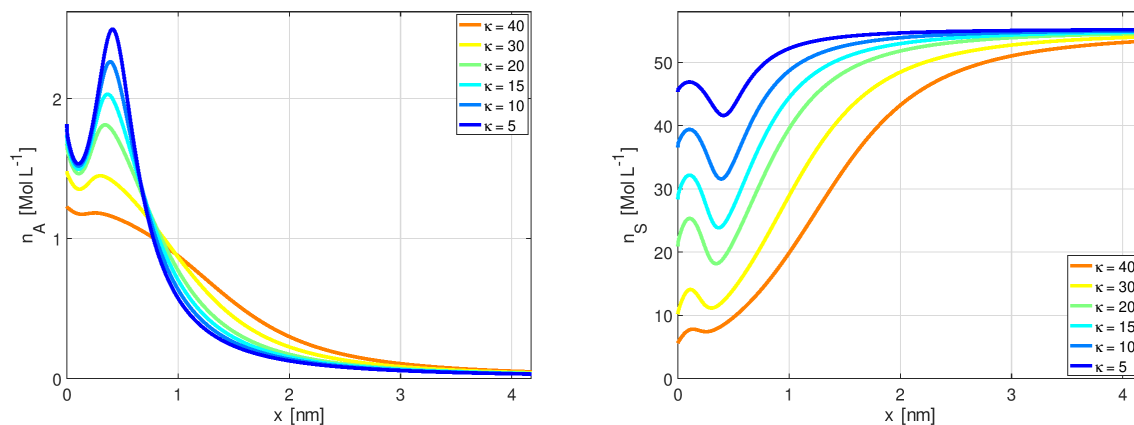


Figure 20: Profiles of the number densities in the boundary layer for $a = 0.01$ and various values of κ .

Again in turn, this yields a larger electric field, which even further decreases the susceptibility (dielectric decrement - field), whereby it becomes favorable for ionic species to not accumulate closer at the interface. Due to the incompressibility, this enforces solvent molecules to remain close at the interface, yielding the non-monotone behavior for n_S and n_A . The non-monotonicity vanishes for either dominant field dependence $a > 0.05$ or negligibly small field dependence. Note, however, that $\varphi(x)$ remains always monotone, even if the n_α become non-monotone.

Expectably, this effect of non-monotonicity is itself again dependent on the solvation number κ , which is shown in Fig. 20 and displays a decline of the hump with increasing numbers of κ (in addition to a broadening of the layer).

However, transitioning from $a_S = a_C = a_S = a$, *i.e.* equal values for species specific electric field dependency, to $a_C = a_A = r_a \cdot a_S$, where the ratio r_a is now varied (*c.f.* section 4.4), *i.e.* different values for the solvent specific electric field dependency of χ than the ionic ones, impacts again the monotonic behavior of n_α (and also χ). Numerical simulations for different values of r_a are shown in Fig. 21.

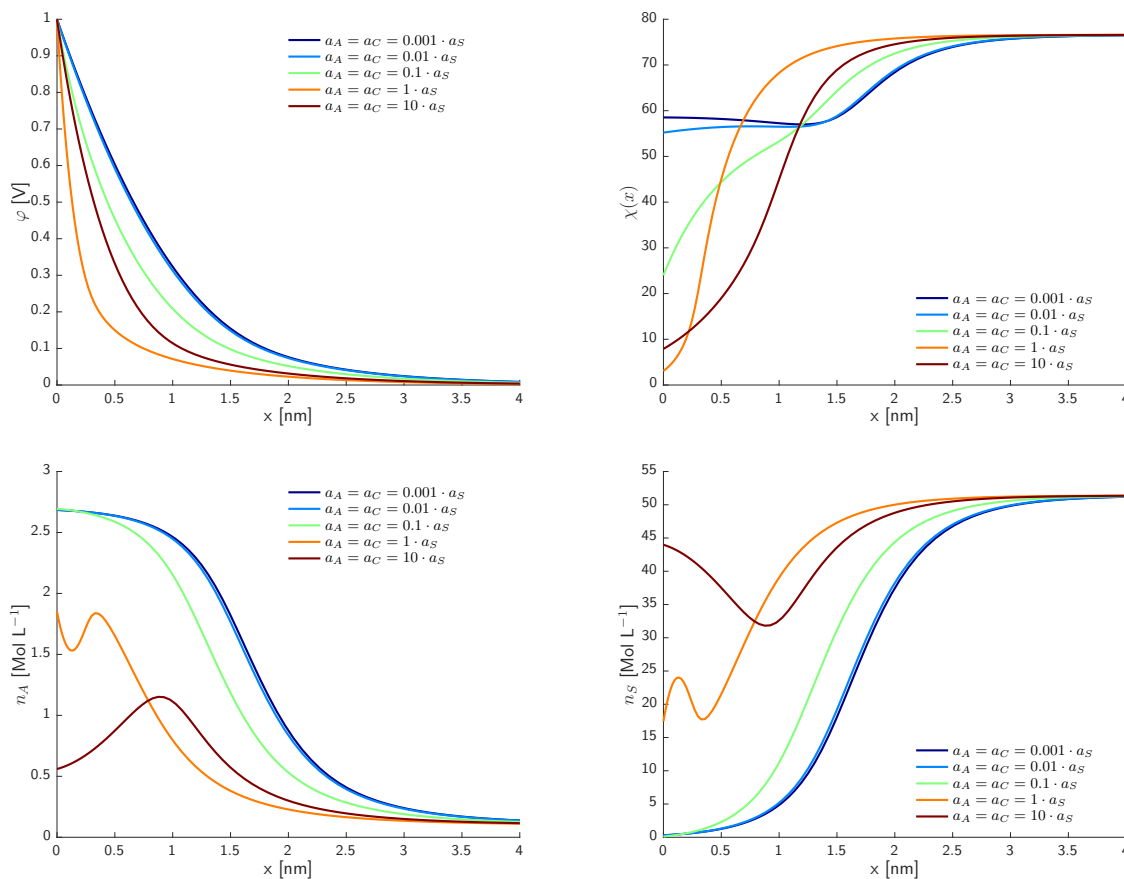


Figure 21: Profiles in the boundary layer for field and concentration dependent susceptibility χ for $\kappa = 20$ and various values of r_a with $a_C = a_A = r_a \cdot a_S$ at an applied voltage of $U = 1V$.

The impact of a larger values for the ionic contribution $a_A = a_C$ to the electric field dependency than the solvent impact a_S yields again a qualitative change from a double hump ($r_a = 1$) to a single hump ($r_a = 10$). If r_a is far smaller than 1, the non-monotonic behavior vanishes.

Differential capacitance. In Fig. 22 we observe that the field dependent susceptibility has an impact on the height of the capacity maxima of the interface. When a gets larger, the height of the maxima decreases for fixed bulk concentration and solvation number. At $a = 0.01$ and $\kappa = 20$, the maximal capacitance is about $90 \mu\text{Fcm}^{-2}$, what is considerably larger than typical observations in experiments.

Varying the solvation number κ , we observe the expected decrease of the capacitance maxima when increasing κ , as it is already known from the case of constant χ .

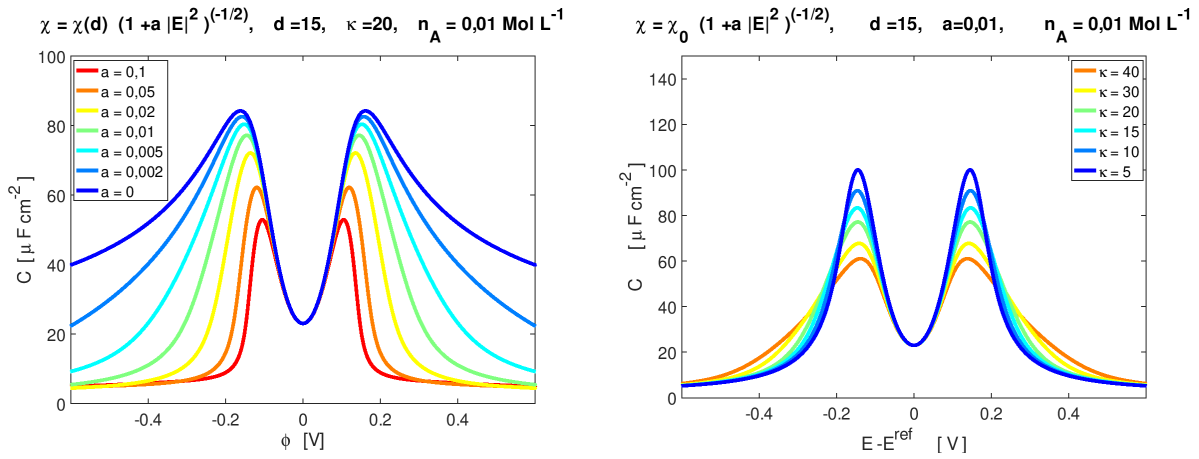


Figure 22: Differential capacitance for a bulk electrolyte χ_0 concentration of 0.01 mol L^{-1} . Left: impact of varying the parameter a , where $a = 0$ corresponds to the constant χ . Right: field dependent $\chi(|E|)$ with $a = 0.01$ for various values of κ .

5.4 Incomplete dissociation.

Incomplete dissociation results in a lower amount of free charge carriers, compared with the fully dissociated case. Nevertheless, the impact of the incomplete dissociation on the capacitance maxima is not very pronounced, unless for larger bulk concentrations large values of the solvation number in the order of $\kappa = 40$ are considered. This is because the saturation level of the ions are determined by the ion size v_α^E in the incompressible mixture and the susceptibility χ as discussed above.

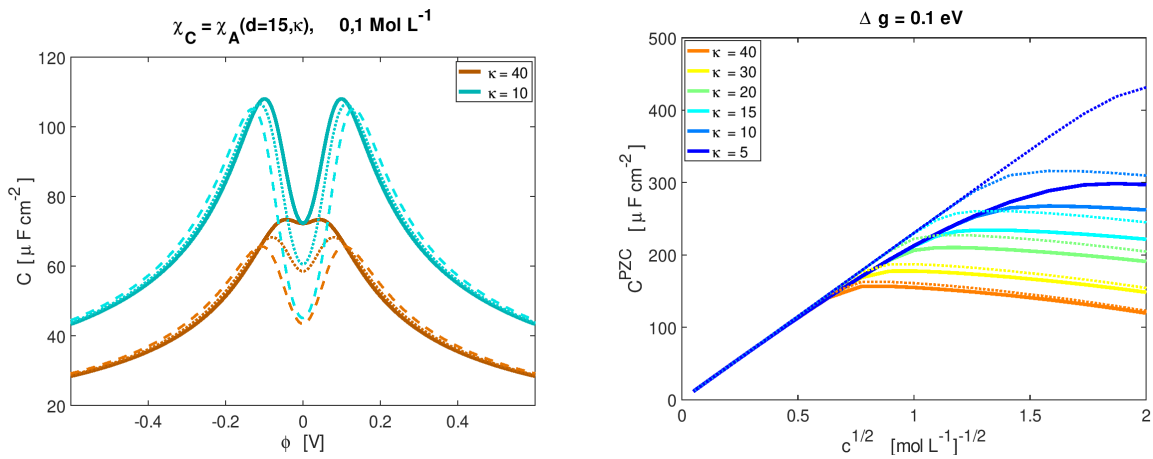


Figure 23: Left: dependence of the capacitance on the dissociation degree. Almost complete dissociation for $\Delta g = 1 \text{ eV}$ (solid lines), and for comparison $\Delta g = -0.15 \text{ eV}$ (dotted), $\Delta g = -0.2 \text{ eV}$ (dashed). Right: capacitance at the PZC susceptibility over bulk concentration for different κ (solid lines). For comparison $\chi = \chi_S = 80$ (dotted lines).

However, the height of the local capacitance minimum at the PZC is reduced as the dissociation degree δ decreases. It can be shown, that –even for the full model with finite ion size and variable susceptibility–

the capacitance at the PZC is determined by the Gouy-Chapman model, viz.

$$\text{at PZC:} \quad C^{\text{BL}} = -\sqrt{2 \frac{(1 + \chi(c)) \varepsilon_0 e_0^2}{k_B T} \cdot \delta(c) c}. \quad (5.2)$$

Thus for given bulk concentration c , the capacitance is determined by $\chi(c)$ and $\delta(c)$ which in turn are controlled by d , κ and Δg . In Fig. 23, we observe that the capacitance at the PZC branches off from the $c^{1/2}$ curve more early for larger κ . For large values of κ , the additional impact of the concentration dependence of χ becomes small. Another consequence of (5.2) is that from a given bulk concentration and measured capacitance at the PZC, the combination $(1 + \chi(c)) \delta(c)$ can be determined.

6 Conclusions

Although the dependence of the dielectric susceptibility on the electric field strength and the electrolyte concentration is well known, it is often neglected in mathematical models for electrolytic solutions. With the analysis carried out in this work, it is evident, however, that the modeling of electrochemical interfaces loses several relevant effects if the dielectric susceptibility is simplified to a constant parameter.

For a consistent thermodynamic treatment of a non-constant susceptibility, one is well advised to reiterate the the modeling process from scratch, *i.e.* beginning with the general balance equations of for matter and electric fields and re-evaluate the entropy principle, but with particular focus on the non-constant susceptibility.

Concentration dependence of χ causes a field dependence of chemical potentials, that in turn affects the mode at different places. The coupling of mixture mechanics with electrodynamics is not a standard straight forward task and special attention is needed in relation with the momentum balance. While the notion of the total stress tensor is unambiguous, it is not obvious how electric field induced contributions to the pressure are treated in consistent manner that is needed in the subtle interplay of the momentum balance and the Poisson equation in extended diffusional equilibrium.

With respect to the field dependence, we emphasize that particular attention is required, in order not to violate the ellipticity condition of the Poisson equation, as it happens e.g. for the approach by [27] and widely adopted in the literature if $m > 1/2$ is chosen. Considering the concentration dependence of χ , we propose a simple approach that is linear the species concentrations of the electrolyte. This fits well with the experimentally observed linear dielectric decrement in the range of not too strongly concentrated electrolytes. Instead of adding higher order nonlinear terms to χ , we propose to treat the dielectric decrement in the concentrated electrolyte by a nonlinear reaction equation for the incomplete dissociation into ions. If we treat the solvation number κ of the ions as a parameter determining the ionic specific volume, then high values of κ strongly limit the possible reduction of χ due to the dielectric decrement.

From our numerical studies, we observe that concentration dependent dielectric decrement only slightly reduces the double layer width but for smaller parameters κ it may strongly change the qualitative behavior of boundary layers as it reduces the saturation level of counter-ions and thereby prevents the complete removal of the solvent from the interface. While it is in principle possible to treat strongly charged boundary layers by a constant "effective" susceptibility, we remark that this χ^{eff} may actually smaller than the minimum of the the concentration dependent χ obtained in an equally charged layer.

From the numerical study of field dependent dielectric saturation, we observe that the boundary layer

width may be strongly reduced depending on the strength of the field dependence. Thereby the ability of the layer to store charge may abruptly break down.

A combination of field and concentration dependency can in addition cause completely new qualitative behavior of the boundary layer, such as non-monotonous profiles of the ion concentrations.

Similar as in the case of other steric modified Poisson-Boltzmann models the parameter determining ion size, in our case this is in an indirect way the solvation number κ , determines the height of the local maxima in the differential capacitance. Similar to previous studies in the literature, we find that both dependencies of χ have the tendency to allow the deduction of lower values of the size parameter from the fit to experimental data.

A Appendix

A.1 Material model for the free energy density $\rho\psi^{\text{mat}}$

We consider $\rho\psi^{\text{mat}}$ as superposition of (i) a reference contribution

$$\rho\psi^{\text{Ref}} = \sum_{\alpha \in \mathcal{I}} n_{\alpha} \psi_{\alpha}^{\text{E}}, \quad (\text{A.1})$$

where ψ_{α}^{E} are the free energy densities of the pure substances, (ii) an entropy of mixing contribution

$$\rho\psi^{\text{Mix}} = k_B T \sum_{\alpha \in \mathcal{I}} n_{\alpha} \ln \left(\frac{n_{\alpha}}{n} \right), \quad \text{with } n = \sum_{\alpha \in \mathcal{I}} n_{\alpha}, \quad (\text{A.2})$$

accounting for the entropy gain of composition and solvation effects [17], and (iii) a mechanical contribution

$$\rho\psi^{\text{Mech}} = (p^R - K) \left(\sum_{\alpha \in \mathcal{I}} v_{\alpha}^{\text{E}} n_{\alpha} - 1 \right) + K \left(\sum_{\alpha \in \mathcal{I}} v_{\alpha}^{\text{E}} n_{\alpha} \right) \ln \left(\sum_{\alpha \in \mathcal{I}} v_{\alpha}^{\text{E}} n_{\alpha} \right), \quad (\text{A.3})$$

accounting for different molar volumes v_{α}^{E} of the species and respective contribution to the volume (or pressure). Additional contributions, such as an enthalpy of mixing or Debye–Hückel terms, can in principle be considered in this framework, however, are not considered in this work.

We have thus $\rho\psi^{\text{mat}} = \rho\psi^{\text{Ref}} + \rho\psi^{\text{Ent}} + \rho\psi^{\text{Mech}}$ and seek the limit $K \rightarrow \infty$ of the compression modulus since we want to model the electrolyte as incompressible liquid. This implies several aspects [34],

- 1 a variable transformation $(n_0, \dots, n_N) \rightarrow (p, y_1, \dots, y_N)$, where y_{α} are the mole fractions

$$y_{\alpha} = \frac{n_{\alpha}}{n} \quad \text{with} \quad \sum_{\alpha \in \mathcal{I}} y_{\alpha} = 1, \quad (\text{A.4})$$

- 2 the incompressibility constraint

$$\sum_{\alpha \in \mathcal{I}} v_{\alpha}^{\text{E}} n_{\alpha} = 1, \quad (\text{A.5})$$

which yields the representations

$$q = e_0 \frac{\sum_{\alpha \in \mathcal{I}} z_{\alpha} y_{\alpha}}{\sum_{\alpha \in \mathcal{I}} v_{\alpha}^{\text{E}} y_{\alpha}}, \quad \chi = \frac{\sum_{\alpha \in \mathcal{I}} \chi_{\alpha} v_{\alpha}^{\text{E}} y_{\alpha}}{\sum_{\alpha \in \mathcal{I}} v_{\alpha}^{\text{E}} y_{\alpha}}. \quad (\text{A.6})$$

3 and that mechanical contribution of the chemical potential becomes linear in the pressure, *i.e.*

$$\mu_{\alpha}^{\text{mat}} \propto v_{\alpha}^{\text{E}} \cdot p. \quad (\text{A.7})$$

We emphasize that the incompressibility is a not a necessary, but useful assumption for the scope of this work. Compressible mixtures can similiarly be treated if the chemical potential functions and the corresponding pressure-volume relations are consistently derived.

A.2 Non-dimensionalization.

For the further (numerical) calculations it is convenient to introduce non-dimensional variables. We consider

$$\frac{x}{\lambda} \rightarrow x \quad \lambda \frac{e_0}{k_B T} E \rightarrow E \quad (\text{A.8})$$

$$\frac{e_0}{k_B T} (\varphi - \varphi^{\text{bulk}}) \rightarrow \varphi \quad \frac{v_{\alpha}}{v_0} \rightarrow v_{\alpha} \quad (\text{A.9})$$

$$\frac{v_0}{k_B T} (p - p^{\text{bulk}}) \rightarrow p \quad \frac{v_0}{e_0} q \rightarrow q \quad (\text{A.10})$$

$$(\text{A.11})$$

which yields

$$y_{\alpha} = y_{\alpha}^{\text{bulk}} \cdot e^{-z_{\alpha}\varphi - v_{\alpha}p + \eta\chi_{\alpha}v_{\alpha}\frac{1}{2}E^2} \quad (\text{A.12})$$

with

$$\eta := \frac{v_0 \varepsilon_0 (k_B T)^2}{k_B T e_0^2} \cdot \lambda^{-2}. \quad (\text{A.13})$$

The length scale λ of the double layer is in the order of nm, *i.e.* we set $\lambda := 10^{-9}$ [m] and ³ and compute $\eta = 4.2538 \cdot 10^{-5}$. The momentum balance and the Poisson equation non-dimensionalizes as

$$\partial_x p = qE + \eta \cdot \chi \cdot \partial_x (E^2), \quad (\text{A.14})$$

$$\eta \partial_x ((1 + \chi)E) = q \quad (\text{A.15})$$

$$\partial_x \varphi = -E. \quad (\text{A.16})$$

Note that only a single scaling paramter η is present in coupled equation system (A.12), (A.14), (A.14).

A.3 Derivation of the two-point boundary value problem

Two-point boundary value problem. In order to compute the spatially resolved space charge layers, which are responsible for the boundary layer charge Q , we derive the corresponding two-point boundary value problem and a representation which is solvable with standard numerical tools.

³ v_0 corresponds here to the value of water, *i.e.* $(v_0)^{-1} = 55.4 \text{ mol L}^{-1} = 55.4 \text{ mol}10^3 \text{ m}^{-3}$ whereby $v_0 = 1.8051 \cdot 10^{-5} \text{ m}^3 \text{ mol}^{-1}$

In order to use standard numerical solvers for two-point boundary value problems, it is necessary to rewrite (A.14)–(A.16) as first order non-linear ODE system $\vec{z}' = \vec{f}(\vec{z})$. We obtain

$$\partial_\xi \varphi = -E \quad (\text{A.17})$$

$$\partial_\xi E = f_1(\varphi, p, E) \quad \text{with} \quad f_1(\varphi, p, E) := \frac{q(1 - \eta\chi_p \cdot E^2) + \eta\chi_\varphi E^2}{\eta((1 + \chi) + \chi_E \cdot E + \eta\chi_p\chi E^2)} \quad (\text{A.18})$$

$$\partial_\xi p = f_2(\varphi, p, E) \quad \text{with} \quad f_2(\varphi, p, E) := q \cdot E + \eta\chi E f_1(\varphi, p, E). \quad (\text{A.19})$$

Together with the boundary conditions

$$\varphi|_{x=0} = \frac{e_0}{k_B T} \cdot U, \quad p|_{x=x^{\text{bulk}}} = 0, \quad E|_{x=x^{\text{bulk}}} = 0, \quad (\text{A.20})$$

we have thus a two-point boundary value problem (BVP) which can be solved numerically. Note that the numerical strategy to solve such a coupled, highly non-linear ODE system exploits an iterative *charging* of the interface, where $U = k \cdot \Delta U = U_k$, and for instance $\Delta U = 0.01$ [V] and $k = 0, 1, \dots, 100$. A numerical solution at U_k is then denoted as $(\tilde{\varphi}_k, \tilde{p}_k, \tilde{E}_k)$ and serves as initial value for the non-linear solver of BVP at U_{k+1} .

For the two cases of a *Concentration dependent susceptibility* (Case 2, (2.40a)) and *Concentration and electric field dependent susceptibility* (Case 3, (2.41)) we provide explicit representations for f_1 and f_2

Concentration dependent susceptibility - Completely dissociated electrolyte AC For an electrolyte consisting only of cations and anions, we provide here the explicit functions to determine f_1 and f_2

$$y_\alpha = y_\alpha^E \cdot e^{-z_\alpha \varphi - v_\alpha p + \delta \chi_\alpha v_\alpha \frac{1}{2} E^2} \quad (\text{A.21})$$

$$y_0 = 1 - y_A - y_C \quad (\text{A.22})$$

$$h := 1 + (v_A - 1)y_A + (v_C - 1)y_C \quad (\text{A.23})$$

$$q = \frac{z_A y_A + z_C y_C}{h} \quad (\text{A.24})$$

$$g := 1 + \nu_A y_A + \nu_C y_C \quad \text{with} \quad \nu_\alpha := v_\alpha \frac{\chi_\alpha}{\chi_0} - 1, \alpha = A, C \quad (\text{A.25})$$

$$\chi = \chi_0 \frac{g}{h} \quad (\text{A.26})$$

$$\partial_p y_\alpha = -v_\alpha y_\alpha \quad (\text{A.27})$$

$$\partial_p h = -(v_A - 1)v_A y_A - (v_C - 1)v_C y_C =: h_p \quad (\text{A.28})$$

$$\partial_p g = -\nu_A v_A y_A - \nu_C v_C y_C =: g_p \quad (\text{A.29})$$

$$\chi_p = \chi_0 \partial_p \left(\frac{g}{h} \right) = \chi_0 \frac{g_p \cdot h - g \cdot \partial_p h}{h^2} \quad (\text{A.30})$$

$$\partial_\varphi y_\alpha = -z_\alpha y_\alpha \quad (\text{A.31})$$

$$\partial_\varphi h = -z_A (v_A - 1)y_A - z_C (v_C - 1)y_C =: h_\varphi \quad (\text{A.32})$$

$$\partial_\varphi g = -z_A \nu_A y_A - z_C \nu_C y_C =: g_\varphi \quad (\text{A.33})$$

$$\chi_\varphi = \chi_0 \partial_\varphi \left(\frac{g}{h} \right) = \chi_0 \frac{g_\varphi \cdot h - g \cdot h_\varphi}{h^2} \quad (\text{A.34})$$

$$\partial_E y_\alpha = \delta \chi_\alpha v_\alpha \cdot E y_\alpha \quad (\text{A.35})$$

$$\partial_E h = (v_A - 1)\delta\chi_A v_A \cdot E y_A + (v_C - 1)\delta\chi_C v_C \cdot E y_C =: h_E \quad (\text{A.36})$$

$$\partial_E g = \nu_A \delta\chi_A v_A \cdot E y_A + \nu_C \delta\chi_C v_C \cdot E y_C \quad (\text{A.37})$$

$$\chi_E = \chi_0 \partial_E \left(\frac{g}{h} \right) = \chi_0 \frac{g_E \cdot h - g \cdot h_E}{h^2} \quad (\text{A.38})$$

Insertion of the functions $(q, \chi, \chi_\varphi, \chi_p, \chi_E)$ in (A.18) and (A.19) yields explicit functions which can be solved, for instance, with Matlab[®] and the `bvp4c` solver.

Concentration and electric field dependent susceptibility - Completely dissociated electrolyte

AC We consider

$$\rho\psi^{\text{pol}} = -\frac{\varepsilon_0}{2} X \quad \text{with} \quad X = \sum_{\alpha=0}^N v_\alpha^E n_\alpha \chi_\alpha^0 \cdot \underbrace{\left(\frac{2}{a_\alpha} \sqrt{1 + a_\alpha |\mathbf{E}|^2} \right)}_{=: X_\alpha} = \sum_{\alpha=0}^N v_\alpha^E n_\alpha, \quad (\text{A.39})$$

which yields

$$\mu_\alpha^{\text{pol}} = -v_\alpha^E \cdot \frac{\varepsilon_0}{2} X_\alpha(E^2) \quad (\text{A.40})$$

and

$$\chi = \frac{\partial X}{\partial E^2} = \sum_{\alpha=0}^N v_\alpha^E n_\alpha \underbrace{\chi_\alpha^0 \cdot (1 + a_\alpha |\mathbf{E}|^2)^{-\frac{1}{2}}}_{:= \chi_\alpha(E^2)} \quad (\text{A.41})$$

For an electrolyte consisting only of cations and anions, we provide here the explicit functions to determine f_1 and f_2

$$y_\alpha = y_\alpha^E \cdot e^{-z_\alpha \varphi - v_\alpha p + \delta v_\alpha \frac{1}{2} X_\alpha(E^2)} \quad (\text{A.42})$$

$$y_0 = 1 - y_A - y_C \quad (\text{A.43})$$

$$h := 1 + (v_A - 1)y_A + (v_C - 1)y_C \quad (\text{A.44})$$

$$q = \frac{z_A y_A + z_C y_C}{h} \quad (\text{A.45})$$

$$g := \chi_0 + \nu_A y_A + \nu_C y_C \quad \text{with} \quad \nu_\alpha := v_\alpha \chi_\alpha - \chi_0, \alpha = A, C \quad (\text{A.46})$$

$$\chi = \frac{g}{h} \quad (\text{A.47})$$

pressure derivatives (A.48)

$$\partial_p y_\alpha = -v_\alpha y_\alpha \quad (\text{A.49})$$

$$\partial_p h = -(v_A - 1)v_A y_A - (v_C - 1)v_C y_C =: h_p \quad (\text{A.50})$$

$$\partial_p g = -\nu_A v_A y_A - \nu_C v_C y_C =: g_p \quad (\text{A.51})$$

$$\chi_p = \partial_p \left(\frac{g}{h} \right) = \frac{g_p \cdot h - g \cdot \partial_p h}{h^2} \quad (\text{A.52})$$

potential derivatives (A.53)

$$\partial_\varphi y_\alpha = -z_\alpha y_\alpha \quad (\text{A.54})$$

$$\partial_\varphi h = -z_A (v_A - 1)y_A - z_C (v_C - 1)y_C =: h_\varphi \quad (\text{A.55})$$

$$\partial_\varphi g = -z_A \nu_A y_A - z_C \nu_C y_C =: g_\varphi \quad (\text{A.56})$$

$$\chi_\varphi = \partial_\varphi \left(\frac{g}{h} \right) = \frac{g_\varphi \cdot h - g \cdot h_\varphi}{h^2} \quad (\text{A.57})$$

field derivatives (A.58)

$$\partial_E X_\alpha(E^2) = \partial_{E^2} X_\alpha 2E = \chi_\alpha 2E \quad (\text{A.59})$$

$$\partial_E \chi_\alpha = -\frac{1}{2} \chi_\alpha^0 \cdot (1 + a_\alpha E^2)^{-\frac{3}{2}} \cdot 2a_\alpha E = -\chi_\alpha^0 \cdot (1 + a_\alpha E^2)^{-\frac{3}{2}} a_\alpha E =: \theta_\alpha \quad (\text{A.60})$$

$$\partial_E y_\alpha = y_\alpha \delta v_\alpha \chi_\alpha \cdot E \quad (\text{A.61})$$

$$\partial_E h = (v_A - 1) \delta \chi_A v_A \cdot E y_A + (v_C - 1) \delta \chi_C v_C \cdot E y_C =: h_E \quad (\text{A.62})$$

$$\partial_E \nu_\alpha = v_\alpha \theta_\alpha - \theta_0 =: \eta_\alpha \quad (\text{A.63})$$

$$\partial_E g = \theta_0 + \nu_A \delta \chi_A v_A \cdot E y_A + \nu_C \delta \chi_C v_C \cdot E y_C + \eta_A y_A + \eta_C y_C =: g_E \quad (\text{A.64})$$

$$\chi_E = \partial_E \left(\frac{g}{h} \right) = \frac{g_E \cdot h - g \cdot h_E}{h^2} \quad (\text{A.65})$$

Insertion of the functions $(q, \chi, \chi_\varphi, \chi_p, \chi_E)$ in (A.18) and (A.19) yields explicit functions which can be solved, for instance, with Matlab[®] and the `bvp4c` solver.

A.4 Algebraic solution

To evaluate χ^{surf} , which can be written as

$$\chi^{\text{surf}} = \frac{\sum_{\alpha \in \mathcal{I}} \chi_\alpha v_\alpha^E y_\alpha^{\text{surf}}}{\sum_{\alpha \in \mathcal{I}} v_\alpha^E y_\alpha^{\text{surf}}} \quad (\text{A.66})$$

and to determine p^{surf} , we employ the following strategy. We seek a non-linear algebraic equation system $\mathbf{g}(y_1^{\text{surf}}, \dots, y_N^{\text{surf}}, p^{\text{surf}}; U) = \mathbf{0}$, which parametrically depends on U and allows us thus to determine $y_\alpha^{\text{surf}} = \check{y}_\alpha^{\text{surf}}(U)$, $p^{\text{surf}} = \check{p}^{\text{surf}}(U)$ as (numerical) solution of $\mathbf{g} = \mathbf{0}$.

Insertion of the representation (2.61) and evaluation at $x = 0$ actually yields for $\alpha = 1, \dots, N$

$$y_\alpha^{\text{surf}} - y_\alpha^{\text{bulk}} \cdot e^{-\frac{e_0 z_\alpha}{k_B T} U - \frac{v_\alpha^E}{k_B T} \left(1 - \frac{\chi_\alpha}{1 + 2\chi^{\text{surf}}}\right) p^{\text{surf}}} =: g_\alpha(y_1^{\text{surf}}, \dots, y_N^{\text{surf}}, p^{\text{surf}}; U) \stackrel{!}{=} 0, \quad (\text{A.67})$$

where y_0 is replaced by $y_0 = 1 - \sum_{\alpha=1}^N y_\alpha$ everywhere. However, we have additionally the constraint

$$1 - \sum_{\alpha=1}^N y_\alpha^{\text{surf}} - y_0^{\text{bulk}} \cdot e^{-\frac{v_0^E}{k_B T} \left(1 - \frac{\chi_0}{1 + 2\chi^{\text{surf}}}\right) p^{\text{surf}}} =: g_{N+1}(y_1^{\text{surf}}, \dots, y_N^{\text{surf}}, p^{\text{surf}}; U) \quad (\text{A.68})$$

whereby $\mathbf{g} \in \mathbb{R}^{N+1}$. Hence we can write

$$Q = -\text{sign}(\varphi - \varphi^{\text{bulk}}) \sqrt{\frac{\check{p}^{\text{surf}}(U) - p^{\text{bulk}}}{\varepsilon_0 \left(\frac{1}{2} + \check{\chi}^{\text{surf}}(U)\right)}} =: \check{Q}(U). \quad (\text{A.69})$$

which yields a semi-explicit expression for the boundary layer charge Q as function of the applied voltage U .

References

- [1] R.M. Adar, T. Markovich, A. Levy, H. Orland, and D. Andelman. Dielectric constant of ionic solutions: Combined effects of correlations and excluded volume. *J. Chem. Phys.*, 149(5):054504, 2018.

- [2] A. Apelblat and E. Manzurola. Volumetric properties of water, and solutions of sodium chloride and potassium chloride at temperatures from $T = 277.15K$ to $T = 343.15K$ at molalities of (0.1, 0.5, and 1.0) $mol \cdot kg^{-1}$. *J. Chem. Thermodyn.*, 31(7):869–893, 1999.
- [3] M. Z. Bazant, K. Thornton, and A. Ajdari. Diffuse-charge dynamics in electrochemical systems. *Phys. Rev. E*, 70:021506, 2004.
- [4] M.Z. Bazant, M.S. Kilic, B.D. Storey, and A. Ajdari. Towards an understanding of induced-charge electrokinetics at large applied voltages in concentrated solutions. *Adv. Colloid Interface Sci.*, 152(1):48–88, 2009.
- [5] R. Becker and F. Sauter. *Theorie der Elektrizität*, volume 1. Teubner, Stuttgart, 1973.
- [6] D. Ben-Yaakov, D. Andelman, and R. Podgornik. Dielectric decrement as a source of ion-specific effects. *J. Chem. Phys.*, 134(7):074705, 2011.
- [7] P. Berg and B.E. Benjaminsen. Effects of finite-size ions and relative permittivity in a nanopore model of a polymer electrolyte membrane. *Electrochim. Acta*, 120:429–438, 2014.
- [8] J.O'M. Bockris, A.K.N. Reddy, and M.E. Gamboa-Aldeco. *Modern Electrochemistry 2A: Fundamentals of Electrodicts*. Kluwer, New York, 2000.
- [9] F. Booth. The dielectric constant of water and the saturation effect. *The Journal of Chemical Physics*, 19(4):391–394, 1951.
- [10] I. Borukhov, D. Andelman, and H. Orland. Steric effects in electrolytes: A modified Poisson–Boltzmann equation. *Phys. Rev. Lett.*, 79:435–438, 1997.
- [11] R. Buchner, G. T. Hefter, and P. M. May. Dielectric relaxation of aqueous NaCl solutions. *The Journal of Physical Chemistry A*, 103(1):1–9, 1999.
- [12] A. Chandra. Static dielectric constant of aqueous electrolyte solutions: Is there any dynamic contribution? *J. Chem. Phys.*, 113(3):903–905, 2000.
- [13] V. B. Chu, Y. Bai, J. Lipfert, D. Herschlag, and S. Doniach. Evaluation of ion binding to dna duplexes using a size-modified poisson-boltzmann theory. *Biophysical Journal*, 93(9):3202 – 3209, 2007.
- [14] I. Danielewicz-Ferchmin and A. R. Ferchmin. Static permittivity of water revisited: ϵ in the electric field above $108Vm^{-1}$ and in the temperature range $273 \leq T \leq 373K$. *Phys. Chem. Chem. Phys.*, 6:1332–1339, 2004.
- [15] P. Debye. *Polar Molecules*. Chemical Catalogue Company, New York, 1929.
- [16] S. R. deGroot and P. Mazur. *Non-equilibrium Thermodynamics*. Dover Publications, New York, 1984.
- [17] W. Dreyer, C. Gohlke, and M. Landstorfer. A mixture theory of electrolytes containing solvation effects. *Electrochem. Commun.*, 43:75–78, 2014.
- [18] W. Dreyer, C. Gohlke, M. Landstorfer, and R. Müller. New insights on the interfacial tension of electrochemical interfaces and the Lippmann equation. *Eur. J. Appl. Math.*, 29(4):708–753, 2018.

- [19] W. Dreyer, C. Gohlke, and R. Müller. Overcoming the shortcomings of the Nernst–Planck model. *Phys. Chem. Chem. Phys.*, 15:7075–7086, 2013.
- [20] W. Dreyer, C. Gohlke, and R. Müller. Bulk-surface electro-thermodynamics and applications to electrochemistry. *Entropy*, 20(12):939, 2018.
- [21] B. Figliuzzi, W.H.R. Chan, C.R. Buie, and J.L. Moran. Nonlinear electrophoresis in the presence of dielectric decrement. *Phys. Rev. E*, 94:023115, Aug 2016.
- [22] R. Fitzpatrick. *Classical electromagnetism*. The University of Texas at Austin, Austin, 2006.
- [23] J. A. Gates and R. H. Wood. Densities of aqueous solutions of sodium chloride, magnesium chloride, potassium chloride, sodium bromide, lithium chloride, and calcium chloride from 0.05 to 5.0 mol · kg⁻¹ and 0.1013 to 40 MPa at 298.15 K. *J. Chem. Eng. Data*, 30(1):44–49, 1985.
- [24] E. Gongadze and A. Iglič. Asymmetric size of ions and orientational ordering of water dipoles in electric double layer model - an analytical mean-field approach. *Electrochim. Acta*, 178:541 – 545, 2015.
- [25] E. Gongadze, U. van Rienen, and A. Iglič. Generalized Stern models of the electric double layer considering the spatial variation of permittivity and finite size of ions in saturation regime. *Gen Physiol Biophys*, 16(4):576–594, 2011.
- [26] E. Gongadze, U. van Rienen, V. Kralj-Iglič, and A. Iglič. Langevin Poisson-Boltzmann equation: point-like ions and water dipoles near a charged surface. *Gen. Physiol. Biophys.*, 30(2):130–137, 2011.
- [27] D. C. Grahame. Effects of dielectric saturation upon the diffuse double layer and the free energy of hydration of ions. *The Journal of Chemical Physics*, 18(7):903–909, 1950.
- [28] A. Gupta and H.A. Stone. Electrical double layers: Effects of asymmetry in electrolyte valence on steric effects, dielectric decrement, and ion–ion correlations. *Langmuir*, 34(40):11971–11985, 2018.
- [29] A. Hamelin and L. Stoicoviciu. Comments on the inner-layer capacity versus charge density curves. *J. Electroanal. Chem.*, 271(1):15–26, 1989.
- [30] J. B. Hasted, D. M. Ritson, and C. H. Collie. Dielectric properties of aqueous ionic solutions. parts I and II. *J. Chem. Phys.*, 16(1):1–21, 1948.
- [31] M.M. Hatlo, R. van Roij, and L. Lue. The electric double layer at high surface potentials: The influence of excess ion polarizability. *EPL*, 97(2):28010, Jan 2012.
- [32] V. Kralj-Iglič and A. Iglič. A simple statistical mechanical approach to the free energy of the electric double layer including the excluded volume effect. *J. Phys. II*, 6(4):477–491, 1996.
- [33] M. Landstorfer. On the dissociation degree of ionic solutions considering solvation effects. *Electrochemistry Communications*, 92:56 – 59, 2018.
- [34] M. Landstorfer, C. Gohlke, and W. Dreyer. Theory and structure of the metal-electrolyte interface incorporating adsorption and solvation effects. *Electrochim. Acta*, 201:187–219, 2016.
- [35] B. Li. Continuum electrostatics for ionic solutions with non-uniform ionic sizes. *Nonlinearity*, 22(4):811–833, feb 2009.

- [36] J.-L. Liu and B. Eisenberg. Poisson-Nernst-Planck-Fermi theory for modeling biological ion channels. *J. Chem. Phys.*, 141(22):22D532, 2014.
- [37] Y. Marcus. Electrostriction in electrolyte solutions. *Chemical Reviews*, 111(4):2761–2783, 2011.
- [38] Y. Marcus. Evaluation of the static permittivity of aqueous electrolytes. *J. Solution Chem.*, 42(12):2354–2363, 2013.
- [39] J.R. Melcher. *Continuum Electromechanics*. MIT Press, Cambridge, MA, 1981.
- [40] C. W. Monroe. Mechanics of the ideal double-layer capacitor. *J. Electrochem. Soc.*, 167(1):013550, feb 2020.
- [41] I. Müller. *Thermodynamics*. Pitman Publishing, London, 1985.
- [42] Y. Nakayama and D. Andelman. Differential capacitance of the electric double layer: The interplay between ion finite size and dielectric decrement. *J. Chem. Phys.*, 142(4):044706, 2015.
- [43] L. Onsager. Electric moments of molecules in liquids. *J. Am. Chem. Soc.*, 58(8):1486–1493, 1936.
- [44] R. H. Perry and D. W. Green, editors. *Perry's chemical engineers' handbook*. McGraw-Hill, New York, 8 edition, 2008.
- [45] A. Sanfeld. *Introduction to the Thermodynamics of Charged and Polarized Layers*, volume 10 of *Monographs in Statistical Physics and Thermodynamics*. John Wiley & Sons, London, New York, Sydney, 1968.
- [46] W. Schmickler. Double layer theory. *J. Solid State Electrochem.*, 24(9):2175 – 2176, 2020.
- [47] O. Teschke, G. Ceotto, and E. F. de Souza. Interfacial water dielectric-permittivity-profile measurements using atomic force microscopy. *Phys. Rev. E*, 64:011605, Jun 2001.
- [48] C. Truesdell and R. Toupin. *The Classical Field Theories*, volume III/1 of *Handbuch der Physik*. Springer, Berlin, Göttingen, Heidelberg, 1960.
- [49] G. Valette. Double layer on silver single-crystal electrodes in contact with electrolytes having anions which present a slight specific adsorption: Part I. The (110) face. *J. Electroanal. Chem.*, 122:285–297, 1981.